Numerical simulation of shallow water equations and comparison with experimental data

Mikolaj Szydlarski, Chiara Simeoni

Research Report :
numerical simulation of shallow water equations and comparison with experimental data

Mikolaj Szydlarski

Dipartimento di Matematica Pura ed Applicata
Università degli Studi dell'Aquila, Italy
http://www.dm.univaq.it/

Chiara Simeoni

Laboratoire de Mathématiques J.A. Dieudonné
Université Nice Sophia Antipolis, France
http://math.unice.fr/

September 19th, 2007

Contents

List of Figures

Introduction

Computational Fluid Dynamics is a valuable tool for hydraulic engineers. It is used for detailed predictions about what a flow will be for a particular watercourse under certain conditions, without any complicated measurement which can be time consuming and expensive. The demand for efficient and accurate softwares that can deal with the problems faced by hydraulic engineers has lead to numerous commercial packages appearing on the market place. In the past, available softwares required to use powerful computers and long computing times, however the situation is improving with the advances made in computer hardware. In addition, several others areas can be identified where Computational Fluid Dynamics can be improved, especially in developing numerical schemes able to solve specific difficulties when applied to open channel flow problems. For example, the highly irregular geometries of natural rivers can lead to problems to menage the occurrence of mixed regions of flow, like at hydraulic jumps where supercritical to subcritical transitions take place. This deteriorates some numerical methods, resulting in poor results or difficulties to reproduce solutions. To improve this situation, specific numerical techniques are needed for solving the equations which govern open channel flows.

In any modeling situation, the basis to construct a more complex model is to start with a simpler concept and then to extend the ideas within it to include additional information. A number of mathematical models exist that are suitable for modeling open channel flows, ranging from one dimensional Saint Venant equations to the three dimensional Navier-Stokes system. All are based on the same underlying physics and the choice will depend on the problem considered and requirements of the solution. The one dimensional

Saint Venant equations have been considered for the numerical simulations of shallow water flows on complex topography within this report. Although the Saint Venant equations are relatively simple compared to more sophisticated models such as the Navier-Stokes system, they are nevertheless capable of predicting enough information to be practically used. From a validation perspective, a number of standard test cases exist for the Saint Venant equations where analytical solutions are known.

This report goes on to introduce the shallow water equations and the Saint Venant system. In Chapter 1, we start by showing up physical and mathematical basis behind the model, followed by a more deep look at the conservation laws and simple derivation of shallow water equations from isentropic flows. Chapter 2 presents the Riemann problems for shallow water equations. In Chapter 3, the concept of finite volume numerical schemes for the Saint Vanant system is introduced, together with a description of the kinetic approach used to build a particular numerical scheme. Numerical tests are performed and, finally, a description of the program that has been implemented to solve the Saint Venant system in view of comparison with experimental data.

Chapter 1

Physical and Mathematical Modelling

1.1 Physical basis: Open - channel flows

Simply stated, open-channel flow is the flow of a liquid in a conduit with a free surface. There are many practical examples,both artificial (flumes, spillways, canals, weirs, drainage ditches, culverts) and natural (streams, rivers, estuaries, floodplains). This section introduces the elementary analysis of such flows, which are dominated by the effects of gravity.

The presence of the free surface, which is essentially at atmospheric pressure, both helps and hurts the analysis. It helps because the pressure can be taken constant along the free surface, which therefore is equivalent to the hydraulic grade line of the flow. Unlike flow in closed ducts, the pressure gradient is not a direct factor in open- channel flow, where the balance of forces is confined to gravity and friction. But the free surface complicates the analysis because its shape is a priori unknown, the depth profile changes with conditions and must be computed as part of the problem, especially in unsteady problems involving wave motion (in our case, long waves in shallow water phenomena).

An open channel always has two sides and a bottom, where the flow satisfies the no- slip condition. Therefore even a straight channel has a three-dimensional velocity distribution. Some measurements of straight-channel

Figure 1.1: Measured isovelocity contours in typical straight open-channel flows (*From Ref. [9]*)
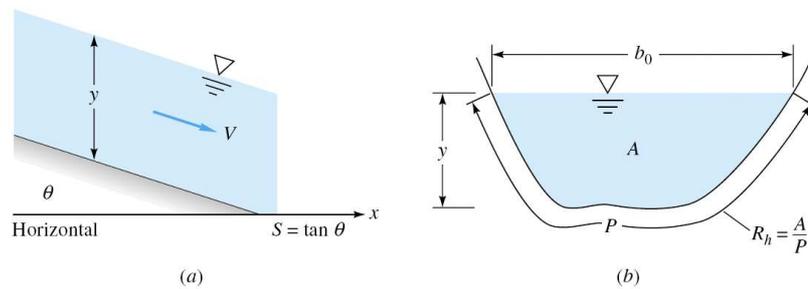
Figure 1.2: Geometry and notation for open-channel flow: *(a)* side view; *(b)* cross section. All these parameters are constant in uniform flow. (*From Ref. [9]*)

velocity contours are shown in Fig (1.1). The profiles are quite complex,with maximum velocity typically occurring in the mid-plane about 20 percent below the surface. In very broad shallow channels the maximum velocity is near the surface, and the velocity profile is nearly logarithmic from the bottom to the free surface. In noncircular channels there are also secondary motions. If the channel curves or meanders, the secondary motion intensifies due to centrifugal effects, with high velocity occurring near the outer radius of the bend. Curved natural channels are subject to strong bottom erosion and deposition effects. With the advent of the supercomputer, it is possible to make numerical simulations of complex flow patterns such as in Fig. (1.1).

However, the practical engineering approach, that is used here, is to make a one-dimensional-flow approximation, as shown in Fig. (1.2). Since

the liquid density is nearly constant, the steady-flow continuity equation reduces to constant-volume flow Q along the channel

$$Q = V(x)A(x) = const \qquad (1.1)$$

where V is average velocity and A the local cross-sectional area, as sketched in Fig. (1.2).

1.1.1 Flow classification by depth variation

The most common method of classifying open-channel flows is by the rate of change of the free-surface depth. The simplest and most widely analyzed case is uniform flow, where the depth (hence the velocity in steady flow) remains constant. Uniform-flow conditions are approximated by long straight runs of constant-slope and constant-area channel.

If the channel slope or cross section changes or there is an obstruction in the flow, then the depth changes and the flow is said to be *varied*. The flow is *gradually varying* if the one-dimensional approximation is valid and *rapidly varying* not. Some examples of this method of classification are shown in Fig. (1.3). The classes can be summarized as follows:

1. Uniform flow (constant depth and slope)

2. Varied flow

   - Gradually varied (one-dimensional)
   - Rapidly varied (multidimensional)

Typically uniform flow is separated from rapidly varying flow by a region of gradually varied flow. Gradually varied flow can be analyzed by a first-order differential equation ,but rapidly varying flow usually requires experimentation or three-dimensional potential theory.

1.1.2 Flow classification by Froude Number, Surface wave speed, Specific Energy and Critical Depth

A second and very interesting classification is by dimensionless Froude number, which for a rectangular or very wide channel takes the form
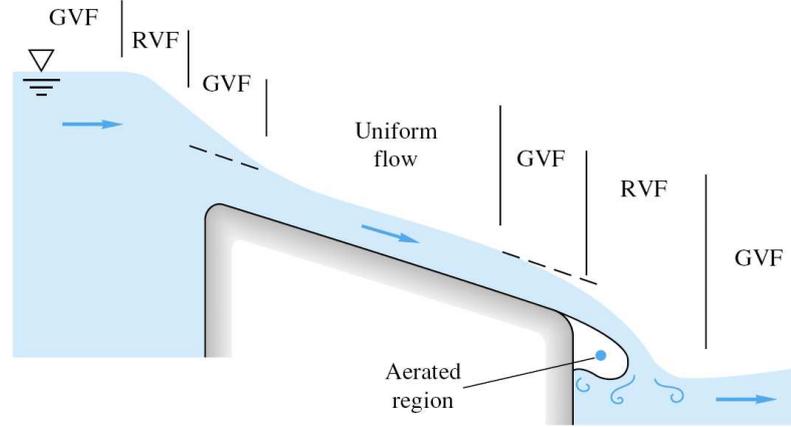
Figure 1.3: Open-channel flow classified by regions of rapidly varyfing flow (RVF), gradually varyfing flow (GVF), and uniform-flow depth profiles. (*From Ref. [9]*)

$Fr = V/(gy)^{1/2}$, where y is the water depth. The three flow regimes are:

$$\begin{aligned} Fr &< 1.0 \quad \text{subcritical flow} \\ Fr &= 1.0 \quad \text{critical flow} \\ Fr &> 1.0 \quad \text{supercritical flow} \end{aligned} \qquad (1.2)$$

The Froude-number denominator $(gy)^{1/2}$ is the speed of an infinitesimal shallow-water surface wave. We can derive this with reference to Fig. (1.4a), which shows a wave of height δy propagating at speed c into still liquid. To achieve a steady-flow inertial frame of reference, we fix the coordinates on the wave as in Fig. (1.4b), so that the still water moves to the right at velocity c.

For the control volume of Fig. (1.4b), the one-dimensional continuity relation is,

$$\delta V = c \frac{\delta y}{y + \delta y}. \qquad (1.3)$$

The velocity change δV induced by a surface wave is small if the wave is "weak", $\delta y \ll y$. If we neglect bottom friction in the short distance across the wave in Fig. (1.4b), the momentum relation is a balance between the

(a) (b)
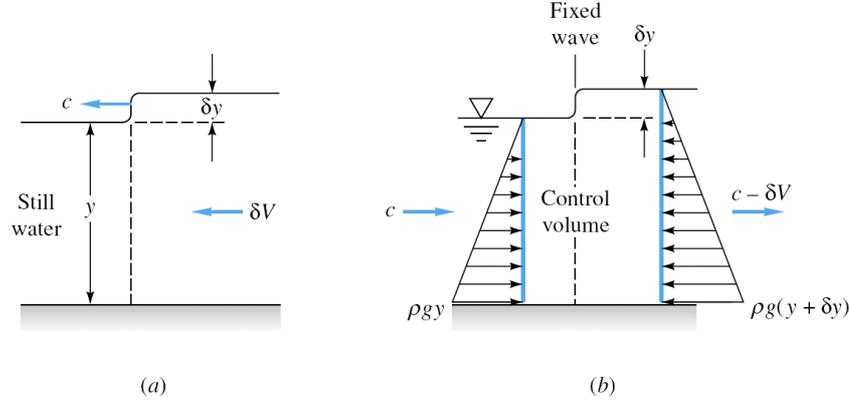
Figure 1.4: Analysis of small surface wave propagating into still shallow water: *(a)* moving wave, nonsteady frame; *(b)* fixed wave, inertial frame of reference. (*From Ref. [9]*)

hydrostatic pressure force and momentum

$$g\left(1 + \frac{1}{2}\frac{\delta y}{y}\right)\delta y = c\delta V. \tag{1.4}$$

By eliminating δV between Eqs. (1.3) and (1.4) we obtain the desired expression for wave propagation speed

$$c^2 = gy\left(1 + \frac{\delta y}{y}\right)\left(1 + \frac{1}{2}\frac{\delta y}{y}\right). \tag{1.5}$$

The "stronger" the wave height δy, the faster the wave speed c. In the limit of an infinitesimal wave height $\delta y \to 0$, the speed becomes:

$$c_0^2 = gy. \tag{1.6}$$

This is the surface-wave equivalent of fluid sound speed, and thus the Froude number in channel flow $Fr = V/c_0$ is the analog of the Mach number.

As in gas dynamics, a channel flow can accelerate from subcritical to critical to supercritical flow and then return to subcritical flow through a sort of normal shock called a *hydraulic jump*. This is illustrated in Fig. (1.5) The flow upstream of the sluice gate is subcritical. It then accelerates to critical and supercritical flow as it passes under the gate,which serves as
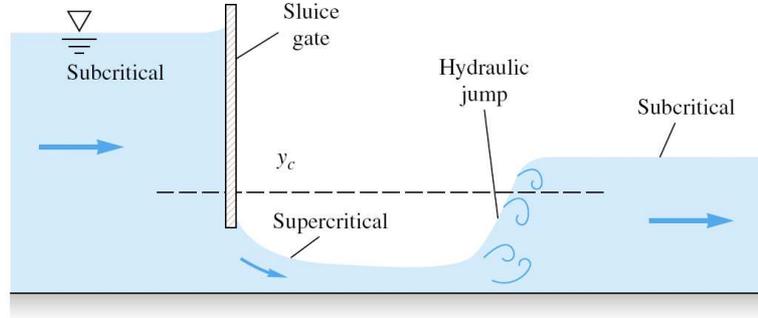
Figure 1.5: Flow under a sluice gate accelerates from subcritical to critical to supercritical flow and then jumps back to subcritical flow. (*From Ref. [9]*)

a sort of "nozzle".Further downstream the flow "shocks" back to subcritical flow because the downstream "receiver" height is too high to maintain supercritical flow.

As suggested by Bakhmeteff[1] in 1911, the specific energy E is a useful parameter in channel flow, it is defined as

$$E = y + \frac{V^2}{2g}.$$

(1.7)

Where y is the water depth. It is seen from Fig. (1.6), that E is the height of the energy grade line (EGL) above the channel bottom. For a given flow rate, there are usually two states possible for the same specific energy. Consider the possible states at a given location. Let $q = Vy$ be the discharge per unit width of a rectangular channel. Then, with q constant, Eq. (1.7) becomes:

$$E = y + \frac{q^2}{2gy^2}.$$

(1.8)

Figure (1.6b) is a plot of y versus E for constant q from Eq. (1.8). There is a minimum value of E at a certain value of y called the *critical depth*. By

---

[1]B.A. Bakhmeteff, *Hydraulics of Open Channels*, McGraw-Hill, New York, 1932
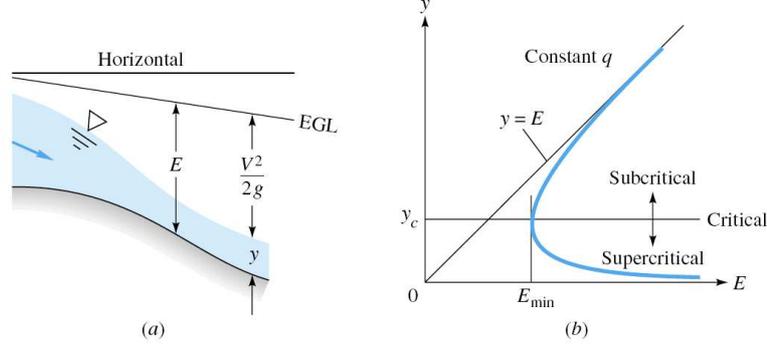
Figure 1.6: Specific-energy considerations: *(a)* illustration sketch; *(b)* depth versus E from Eq. (1.8), showing minimum specific energy occurring at critical depth. (*From Ref. [9]*)

setting $dE/dy = 0$ at constant q, we find that E_{min} occurs at

$$y = y_c = \left(\frac{q^2}{g}\right)^{\frac{1}{3}}. \tag{1.9}$$

The critical depth y_c is sketched as a dashed line in Fig. (1.5) for reference. It is an important parameter in characterizing open-channel flow. The associated energy is:

$$E_{min} = E(y_c) = \frac{3}{2}y_c \tag{1.10}$$

The critical depth y_c corresponds to some critical channel velocity V_c, that turns out to be equal to the shallow-water wave propagation speed c_0 from Eq. (1.6). To see this, we rewrite Eq. (1.9) as

$$q^2 = gy_c^3 = (gy_c)y_c^2 = V_c^2 y_c^2 \tag{1.11}$$

By comparasion it follows that the critical channel velocity is

$$V_c = (gy_c)^{\frac{1}{2}} = c_0, \qquad Fr = 1. \tag{1.12}$$

For $E < E_{min}$ solution does not exists in Fig. (1.6), and thus such a flow is impossible physically. For $E > E_{min}$ solutions are possible: (1) large depth with $V < V_c$, called *subcritical*, and (2) small depth with $V > V_c$, called *supercritical*. In subcritical flow, disturbances can propagate upstream because wave speed $c_0 > V$. In supercritical flow, waves are swept downstream:

Upstream is a zone of silence, and a small obstruction in the flow will create a wedge-shaped wave. The angle of these waves must be

$$\mu = \sin^{-1}\frac{c_0}{V} = \sin^{-1}\frac{(gy^{\frac{1}{2}})}{V} \tag{1.13}$$

The wave angle and the depth can thus be used as a simple measurement of supercritical-flow velocity.

1.1.3 Frictionless Flow over a Bump and Hydraulic Jumps

Now, let us consider a open-channel flow over a bump, as in Fig. (1.7). The behavior of the free surface is sharply different according to whether the approach flow is subcritical or supercritical. The height of the bump also can change the character of the results. For frictionless steady one-dimensional flow, sections 1 and 2 in Fig. (1.7a) are related by continuity and momentum balance:

$$V_1 y_1 = V_2 y_2 \qquad \frac{V_1^2}{2g} + y_1 = \frac{V_2^2}{2g} + y_2 + \Delta h \tag{1.14}$$

Eliminating V_2 between these two gives a cubic polynomial equation for the water depth y_2 over the bump:

$$y_2^3 - E_2 y_2^2 + \frac{V_1^2 y_1^2}{2g} = 0 \qquad \text{where} \qquad E_2 = \frac{V_1^2}{2g} + y_1 - \Delta h \tag{1.15}$$

This equation has one negative and two positive solutions if Δh is not too large. Its behavior is illustrated in Fig. (1.7b) and depends upon whether condition 1 is on the upper or lower leg of the energy curve. The specific energy E_2 is exactly Δh less than the approach energy E_1, and point 2 will lie on the same leg of the curve as E_1. A subcritical approach, $Fr_1 < 1.0$, will cause the water level to decrease at the bump. Supercritical approach flow, $Fr_1 > 1.0$, causes a water-level increase over the bump.

If the bump height reaches $\Delta h_{max} = E_1 - E_c$, as illustrated in Fig. (1.7b), the flow at the crest will be exactly critical ($Fr > 1.0$). If $\Delta h > \Delta h_{max}$, there are no smooth physically correct solutions to Eq. (1.15). That is, a bump too large will "choke" the channel and cause frictional effects, typically a discontinuous solution as a *hydraulic jump* (see Subsection 1.1.3).
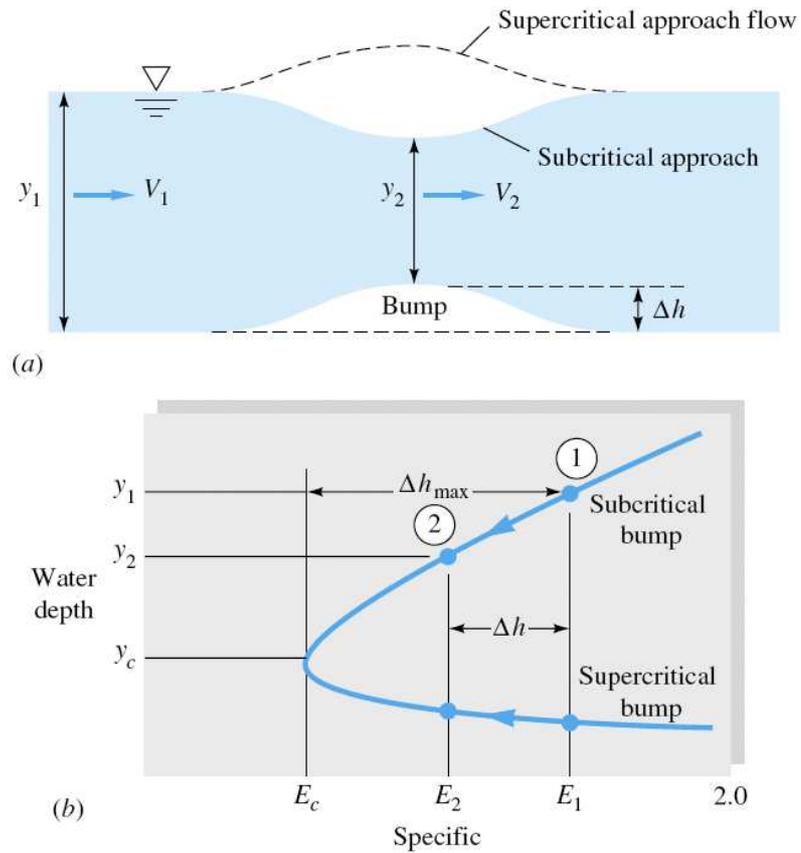
Figure 1.7: Frictionless two-dimensional flow ower a bump: *(a)* definition sketch showing Froude-number dependence; *(b)* specific-energy plot showing bump size and water depths. (*From Ref.* [9])

These bump arguments are reversed if the channel has a *depression* ($\Delta h < 0$): Subcritical approach flow will cause a water-level rise and supercritical flow a fall in depth. Point 2 will be Δh to the right of point 1, and critical flow cannot occur.

In open-channel flow a supercritical flow can change quickly back to a subcritical flow by passing through a hydraulic jump, as in Fig. (1.5). The upstream flow is fast and shallow, and the downstream flow is slow and deep. Unlike the infinitesimally thin normal shock, the hydraulic jump is quite thick, ranging in length from 4 to 6 times the downstream depth y_2.

Being extremely turbulent and agitated, the hydraulic jump is a very effective energy dissipator and is a feature of stilling-basin and spillway applications. Figure (1.8) shows the naturally occurring hydraulic jump formed at the bottom of a river.

The principal parameter affecting hydraulic-jump performance is the upstream Froude number $Fr_1 = V_1/(gy_1)^{\frac{1}{2}}$. The Reynolds number and channel geometry for real flows, have only a secondary effect. The following ranges of operation can be outlined, as illustrated in Fig. (1.9).

Figure 1.8: Naturally occurring hydraulic jump observed on the Upper Spokane Falls north channel (USA). (*Photography from Wikipedia*)
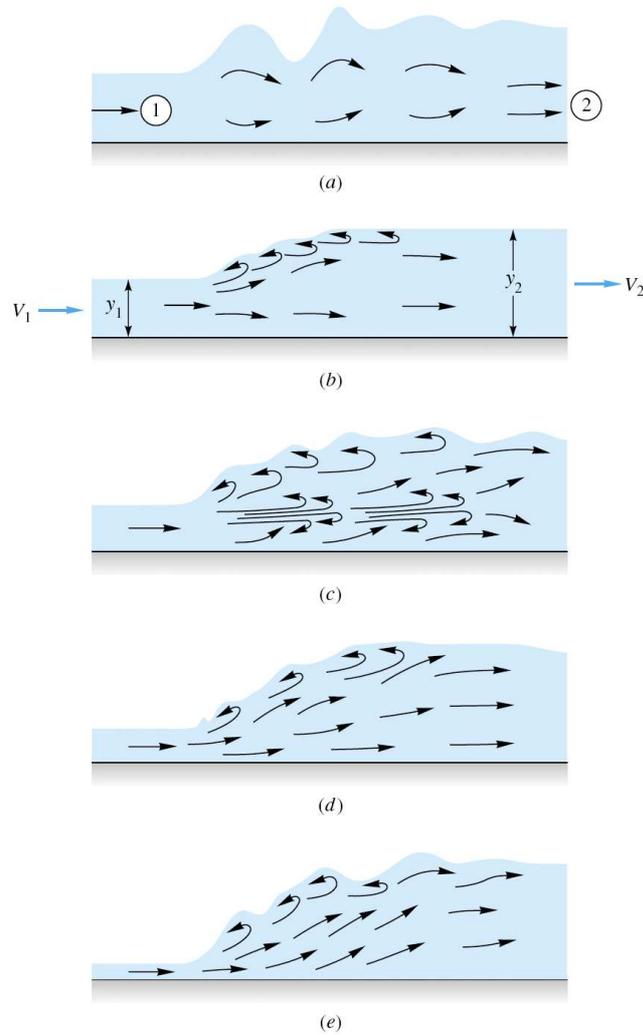
Figure 1.9: Classification of hydraulic jumps: *(a) $Fr = 1.0$ to 1.7: undular jumps; (b) $Fr = 1.7$ to 2.5: weak jumps; (c) $Fr = 2.5$ to 4.5: cillating jumps; (d) $Fr = 4.5$ to 9.0: steady jumps; (e) $Fr > 9.0$: strong jump (From Ref. [9])*

$Fr_1 < 1.0$:   Jump impossible, violates second law of thermo-dynamics.

$Fr_1 = 1.0$ to 1.7:   Standing-wave, or *undular jump* about $4y_2$ long; low dissipation, less than 5%

$Fr_1 = 1.7$ to 2.5:   Smooth surface rise with small rollers, known as a *weak jump*; dissipation 5% to 15%

$Fr_1 = 2.5$ to 4.5:   Unstable, *oscillating jump*; each irregular pulsation creates a large wave which can travel downstream for long distance, damaging earth banks and other structures. Dissipation 15% to 45%.

$Fr_1 = 4.5$ to 9.0:   Stable, well-balanced, steady jump; best performance and action, insensitive to downstream conditions. Best design range. Dissipation 45% to 70%.

$Fr_1 > 9.0$:   Rough, somewhat intermittent strong jump, but good performance. Dissipation 70% to 85%.

A jump which occurs on a steep channel slope can be affected by the difference in water-weight components along the flow. The effect is small, however, so that the classic theory assumes that the jump occurs on a horizontal bottom. We have already analyzed this problem in Sec. (1.1.2) A hydraulic jump is exactly equivalent to the strong fixed wave in Fig. (1.4), where the change in depth δy is not neglected. If V_1 and y_1 upstream are known, V_2 and y_2 are computed by applying continuity and momentum across the wave, as in Eqs. (1.3) and (1.4). Equation (1.5) is therefore the correct solution for a jump if we interpret C and y in Fig. (1.4) as upstream conditions V_1 and y_1, with $C - \delta V$ and $y + \delta y$ being the downstream conditions V_2 and y_2, as in Fig. (1.9) Equation (1.5) becomes:

$$V_1^2 = \frac{1}{2}gy_1\eta(\eta + 1) \qquad (1.16)$$

where $\eta = y_2/y_1$. Introducing the Froude number $Fr_1 = V_1/(gy_1)^{\frac{1}{2}}$ and solving this quadratic equation for η, we obtain:

$$\frac{2y_2}{y_1} = -1 + (1 + 8Fr_1^2)^{\frac{1}{2}} \qquad (1.17)$$

With y_2 thus known, V_2 following form the wide-channel continuity relation:

$$V_2 = \frac{V_1 y_1}{y_2} \tag{1.18}$$

Finally, we can evaluate the dissipation loss across the jump from the steady-flow energy equation:

$$\Delta E = E_1 - E_2 = \left(y_1 + \frac{V_1^2}{2g} \right) \left(y_2 + \frac{V_2^2}{2g} \right) \tag{1.19}$$

Introducing y_2 and V_2 from Eqs. (1.17) and (1.18), we find after considerable algebraic manipulation that:

$$\Delta E = \frac{(y_2 - y_1)^3}{4 y_1 y_2} \tag{1.20}$$

Equation (1.20) shows that the dissipation loss is positive only if $y_2 > y_1$. which is a requirement of the second law of thermodynamic. Equation (1.17) then requires that $Fr_1 > 1.0$; that is, the upstream flow must be supercritical. Finally, Eq. (1.18) shows that $V_2 < V_1$ and the downstream flow is subcritical.

1.2 Systems of conservation laws

Before we pose a model of shallow water, we will focus on systems of conservation laws, as the shallow water equations are a specific case of such systems.

To see how conservation laws arise from physical principles, we will consider the fundamental case of deriving the equation for conservation of mass in a one-dimensional gas dynamic problem, for example the flow in a tube, where properties of the gas such as density and velocity are assumed to be constant across each section of the tube. Then we will show how this gas-model is related with shallow water system.

Let x represents the distance along the tube and let $\rho(x, t)$ be the density of the gas at point x and time t. This density is defined in such way that the total mass of gas in any given section between x_1 and x_2, is given by the integral of density:

$$\text{mass in } [x_1, x_2] \text{ at time } t = \int_{x_1}^{x_2} \rho(x, t) dx \tag{1.21}$$

If we assume that the walls of the tube are impermeable and the mass is neither created nor destroyed, then the mass in one reference section can change only because of gas flowing across the endpoints x_1 or x_2.

Now let $v(x, t)$ be the velocity of the gas at point x and time t, then the rate of flow, (or flux) of gas, past trough this point is given by

$$\text{mass flux at } (x, t) = \rho(x, t) v(x, t). \tag{1.22}$$

By our comments above, the rate of change of mass in $[x_1, x_2]$ is given by the difference in fluxes at x_1 and x_2, namely

$$\frac{d}{dt} \int_{x_1}^{x_2} \rho(x, t) dx = \rho(x_2, t) v(x_2, t) - \rho(x_1, t) v(x_1, t) \tag{1.23}$$

This is one *integral form* of the conservation law. Another form is obtained by integrating (1.23) in time, between t_1 and t_2, giving an expression for the mass in $[x_1, x_2]$ at time $t_2 > t_1$ in terms of the mass at time t_1 and the total

(integrated) flux at each boundary during this time period, that is

$$
\begin{aligned}
\int_{x_1}^{x_2} \rho(x,t_2)dx \;=\; & \int_{x_1}^{x_2} \rho(x,t_1)dx \\
& + \int_{t_1}^{t_2} \rho(x_1,t)v(x_1,t)dt - \int_{t_1}^{t_2} \rho(x_2,t)v(x_2,t)dt.
\end{aligned}
\tag{1.24}
$$

To derive the *differential form* of the conservation law, we must now assume that $\rho(x,t)$ and $v(x,t)$ are differentiable function. Then, using

$$
\rho(x,t_2) - \rho(x,t_1) = \int_{t_1}^{t_2} \frac{\partial}{\partial t}\rho(x,t)dt
\tag{1.25}
$$

and

$$
\rho(x_2,t)v(x_2,t) - \rho(x_1,t)v(x_1,t) = \int_{x_1}^{x_2} \frac{\partial}{\partial x}(\rho(x,t)v(x,t))dx
\tag{1.26}
$$

in (1.24) gives

$$
\int_{t_1}^{t_2}\int_{x_1}^{x_2} \left[\frac{\partial}{\partial t}\rho(x,t) + \frac{\partial}{\partial x}(\rho(x,t)v(x,t)) \right] dxdt = 0.
\tag{1.27}
$$

Since this must hold for any section $[x_1, x_2]$ and over any time interval $[t_1, t_2]$, we conclude that the integrand in (1.27) must be identically zero, i.e.,

$$
\rho_t + (\rho v)_x = 0 \qquad \text{conservation of mass.}
\tag{1.28}
$$

This is the desired *differential form* of the conservation law for mass. The conservation law (1.28) can be solved in isolation only if the velocity $v(x,t)$ is known *a priori* or is known as a function of $\rho(x,t)$. If it is, then ρv is a function of ρ alone, say $\rho v = f(\rho)$, and equation (1.28) becomes a scalar conservation law for ρ,

$$
\rho_t + f(\rho)_x = 0.
\tag{1.29}
$$

More typically equation (1.28) must be solved in conjunction with an equation for the conservation of momentum and energy, and now we simply state them for the case of the *Euler equations* of gas dynamics:

$$
(\rho v)_t + (\rho v^2 + p)_x = 0 \qquad \text{conservation of momentum}
\tag{1.30}
$$

$$(E)_t + (v(E + p))_x = 0 \qquad \text{conservation of energy.} \qquad (1.31)$$

Note that these equations involve another quantity, the pressure p, which must be specified as a given function of ρ, ρv, and E in order for the fluxes to be well defined functions of the conserved quantities alone. This additional, specific equation is called *equation of state* and depends on physical properties of the gas under study.

If we introduce the vector $u \in \mathbb{R}^3$ as

$$u(x,t) = \begin{bmatrix} \rho(x,t) \\ \rho(x,t)v(x,t) \\ E(x,t) \end{bmatrix} \equiv \begin{bmatrix} u_1 \\ u_2 \\ u_3 \end{bmatrix} \qquad (1.32)$$

then the system of equations (1.28), (1.30), (1.31) can be written simply as

$$u_t + f(u)_x = 0 \qquad (1.33)$$

where

$$f(u) = \begin{bmatrix} \rho v \\ \rho v^2 + p \\ v(E + p) \end{bmatrix} = \begin{bmatrix} u_2 \\ \frac{u_2^2}{u_1} + p(u) \\ \frac{u_2(u_3 + p(u))}{u_1} \end{bmatrix}. \qquad (1.34)$$

Again, the form (1.33) is the *differential form* of the conservation laws, which holds in the usual sense only when u is smooth. More generally, the *integral form* for a system of m equations reads

$$\frac{d}{dt} \int_{x_1}^{x_2} u(x,t)dx = f(u(x_2,t)) - f(u(x_1,t)) \qquad (1.35)$$

for all x_1, x_2, t. Equivalently, integrating from t_1 to t_2 gives

$$\begin{aligned} \int_{x_1}^{x_2} u(x,t_2)dx &= \int_{x_1}^{x_2} u(x,t_1)dx \\ &+ \int_{t_1}^{t_2} f(u(x_2,t))dt - \int_{t_1}^{t_2} f(u(x_1,t))dt, \end{aligned} \qquad (1.36)$$

for all x_1, x_2, t_1 and t_2. These integral forms of the conservation law will be fundamental in later analysis.

1.2.1 Euler equations and Isentropic flows

The Euler equations of gas dynamics are a particularly important example because it is closely connected with the shallow water model. The continuity equation (conservation of mass) has been derived in the previous section. Here, we will consider the momentum and energy equation in more detail, as well as the equation of state and a few other quantities of physical (and mathematical) significance, such as the entropy. We will also look at some simplifications namely, the isentropic case, which moves directly to the shallow water model. We "sketch" the derivation here, with an emphasis on the main ideas. A more thorough introduction can be found in Whitham [10].

Recall that ρ is the density, v the velocity, E the total energy, and p the pressure of the gas. The continuity equation is reads

$$\rho_t + (\rho v)_x = 0, \tag{1.37}$$

where the mass flux is given by ρv. More generally, for any quantity z that is advected with the flow there will be a contribution to the flux for z of the form zv. Thus, the momentum equation has a contribution Ev.

In addition to advection, there are forces on the fluid that cause acceleration due to Netwon's laws, and hence changes in momentum. If there are no outside forces, then the only force is due to variations in the fluid itself, and is proportional to the pressure gradient which is simply p_x in one dimension. Combining this with the advective flux gives the momentum equation

$$(\rho v)_t + (\rho v^2 + p)_x = 0. \tag{1.38}$$

The total energy E is often decomposed as

$$E = \frac{1}{2}\rho v^2 + \rho e, \tag{1.39}$$

where the first term is the kinetic energy, while ρe is the internal energy. The variable e, internal energy per unit mass, is called the *specific internal energy* (In general "specific" means "per unit mass"). Internal energy includes rational and vibrational energy and possibly other form of energy in more complicated situations. In Euler equations we assume that the gas is

in chemical and thermodynamic equilibrium and that the internal energy is a known function of pressure and density, that is

$$e = e(p, \rho). \tag{1.40}$$

This is the "equation of state" for the gas, which depends on the particular gas under study.

The total energy advects with the flow, but is also modified due to work done on the system. In the absence of outside forces, work is done only by the pressure forces and is proportional to the gradient in one dimension, of vp. The conservation law for total energy thus takes the following form

$$E_t + [v(E + p)]_x = 0. \tag{1.41}$$

Putting these equations together gives the system of Euler equations

$$\begin{bmatrix} \rho \\ \rho v \\ E \end{bmatrix}_t + \begin{bmatrix} \rho \\ \rho v^2 + p \\ v(E + p) \end{bmatrix}_x = 0. \tag{1.42}$$

We still need to specify the equation of state relating the internal energy to pressure and density. For an ideal gas, internal energy is a function of temperature alone, $e = e(T)$, and T is related to p and ρ by the *ideal gas law*,

$$p = \mathcal{R}\rho T, \tag{1.43}$$

where $\mathcal{R}$ is a constant. To good approximation, the internal energy is simply proportional to the temperature,

$$e = c_v T, \tag{1.44}$$

where c_v is a constant known as the *specific heat at constant volume*. Such gases are called *polytropic*. If energy is added to a fixed quantity of gas, and the volume is held constant, then the change in energy and change in temperature are related via

$$de = c_v dT \tag{1.45}$$

On the other hand, if the gas is allowed to expand while the energy is added, and pressure is held constant instead, not all of the energy goes into

increasing the internal energy. The work done in expanding the volume $1/\rho$ by $d(1/\rho)$ is $pd(1/\rho)$ and we obtain another relation

$$de + pd\left(\frac{1}{\rho}\right) = c_p dT, \tag{1.46}$$

or

$$d\left(e + \frac{p}{\rho}\right) = c_p dT, \tag{1.47}$$

where c_p is a *specific heat at constant pressure*. The quantity

$$h = e + \frac{p}{\rho} \tag{1.48}$$

is called the *enthalpy*. For a polytropic gas, c_p is also assumed to be constant so that (1.47) yields

$$h = c_p T. \tag{1.49}$$

Note that by the ideal gas law,

$$c_p - c_v = \mathcal{R}. \tag{1.50}$$

The equation of state for a polytropic gas turns out to depend only on the *ratio of specific heats*, usually denoted by

$$\gamma = \frac{c_p}{c_v}. \tag{1.51}$$

Internal energy in a molecule is typically split up between various degrees of freedom (translational, rotational, vibrational, etc.). How many degrees of freedom exist depends on the nature of gas. The general *principle of equipartition of energy* says that the avarage energy in each of these is the same. Each degree of freedom contributes an average energy of $\frac{1}{2}kT$ per molecule, where k is *Boltzmann's* constant. This gives a total contribution of $\frac{\alpha}{2}kT$ per molecule if there are α degrees of freedom. Multiplying this by n, the number of molecules per unit mass (which depends on the gas), gives

$$e = \frac{\alpha}{2}nkT. \tag{1.52}$$

The product nk is precisely the gas constant $\mathcal{R}$, so comparing this to (1.44) gives

$$c_v = \frac{\alpha}{2}\mathcal{R} \tag{1.53}$$

From (1.50) we obtain

$$c_p = \left(1 + \frac{\alpha}{2}\mathcal{R}\right), \tag{1.54}$$

and so

$$\gamma = \frac{c_p}{c_v} = \frac{\alpha + 2}{\alpha} \tag{1.55}$$

For monatomic gas the only degrees of freedom are the three translational degrees so $\alpha = 3$ and $\gamma = \frac{5}{3}$. For diatomic gas (such as air, which is composed primarily on N_2 and O_2), there are also two rotational degrees of freedom and $\alpha = 5$, so that $\gamma = \frac{7}{5}$. Note that $T = p/\mathcal{R}\rho$ so that by (1.50) and (1.51),

$$e = c_v T = \left(\frac{c_v}{\mathcal{R}}\right)\frac{p}{\rho} = \frac{p}{(\gamma - 1)\rho}, \quad \text{equation of state for a polytropic gas.} \tag{1.56}$$

Using this in (1.39) gives the common form of the equation of state for a polytropic gas:

$$E = \frac{p}{\gamma - 1} + \frac{1}{2}\rho v^2 \tag{1.57}$$

Another important thermodynamic quantity is the entropy. Roughly speaking, this measures the disorder in the system. The entropy S is defined up to an additive constant by

$$S = c_v \log\left(\frac{p}{\rho^\gamma}\right) + \text{constant.} \tag{1.58}$$

This can be solved for p to give

$$p = \kappa e^{\frac{S}{c_v}}\rho^\gamma, \tag{1.59}$$

where κ is a constant.

From the Euler equations we can derive the following relation

$$S_t + v S_x = 0, \tag{1.60}$$

which says that entropy is constant along particle path in region of smooth flow. In fact (1.60) can be derived from fundamental principles and this equation, together with the conservation of mass and momentum equation, gives an alternative formulation of the Euler equations (though not in conservation form):

$$\begin{aligned} \rho_t + (\rho v)_x &= 0 \\ (\rho v)_t + (\rho v^2 + p)_x &= 0 \\ S_t + v S_x &= 0 \end{aligned} \tag{1.61}$$

It turns out that equation of state then gives p as a function of ρ and S alone, e.g. (1.59) for polytropic gas. In this form the partial derivative of p with respect to ρ (holding S fixed) plays a fundamental role: its square root c is the local *speed of sound* in the gas. For a polytropic gas we have

$$c^2 = \left.\frac{\partial p}{\partial \rho}\right|_{S=\text{constant}} = \gamma \kappa e^{\frac{S}{c_v}} \rho^{\gamma-1} = \gamma \frac{p}{\rho} \tag{1.62}$$

and so

$$c = \sqrt{\frac{\gamma p}{\rho}} \tag{1.63}$$

From our standpoint the most important property of entropy is the fact that is smooth flow entropy remains constant on each particle patch, while if a particle cross a shock then the entropy may jump, but must *increase*. This is the physical entropy condition for shocks. Note that, along a particle path of smooth flow, since S is constant we find by (1.59) that

$$p = \hat{\kappa}\rho^{\gamma}, \tag{1.64}$$

where $\hat{\kappa} = \kappa e^{S/c_v}$ is a constant which depends only on the initial entropy of the particles. This explicit relation between density and pressure along particle paths is sometimes useful. Of course, if the initial entropy varies in space then $\hat{\kappa}$ will be different along different particle paths.

If the entropy is constant everywhere then (1.64) holds with the same value of $\hat{\kappa}$ and the Euler equations simplify. This is the case, for example, if we consider fluid flows that start at uniform rest state (so S is constant) and remains smooth (so S remains constant). Then using (1.64), the equation of state (1.57) reduces to en explicit expression for E in terms of ρ and ρv. The energy equation then becomes redundant and the Euler equations reduce to a system of two equations, the equations of isentropic gas dynamics,

$$\begin{bmatrix} \rho \\ \rho v \end{bmatrix}_t + \begin{bmatrix} \rho v \\ \rho v^2 + \hat{\kappa}\rho^{\gamma} \end{bmatrix}_x = 0. \tag{1.65}$$

1.2.2 Shallow water equations

To derive the one-dimensional shallow water equations, we consider fluid in a channel of unit width and assume that the vertical velocity of the fluid is

negligible and the horizontal velocity $v(x,t)$ is roughly constant throughout any cross section of the channel. This is true if we consider small-amplitude waves in a fluid that is shallow relative to the wavelength. We now assume the fluid is incompressible, so the density $\hat{\rho}$ is constant. Instead we allow the depth of the fluid to vary, and it is this depth, or *height* $h(x,t)$, that we wish to determine. In analogy with (1.21), the total mass in $[x_1, x_2]$ at time t is given by

$$\int_{x_1}^{x_2} \hat{\rho} h(x,t) dx. \tag{1.66}$$

The density of momentum at each point is $\hat{\rho} v(x,t)$, and integrating this vertically gives the mass flux to be $\hat{\rho} v(x,t) h(x,t)$. The constant $\hat{\rho}$ drops out of the conservation of mass equation (1.28), so that we get

$$h_t + (vh)_x = 0 \tag{1.67}$$

The quantity hv is often called *discharge* in shallow water theory, since it measures the rate of water past a point.

The conservation of momentum also takes form as in Euler equations (1.38), namely

$$(\hat{\rho} hv)_t + (\hat{\rho} hv^2 + p)_x = 0, \tag{1.68}$$

but now p is determined from a hydrostatic law, stating that the pressure at distance $h - y$ below the surface is $\hat{\rho} g (h - y)$, where g is the gravitational constant. This pressure arises simply from the weight of the fluid above. Integrating this vertically from $y = 0$ to $y = h(x,t)$ gives the total pressure felt at (x,t), the proper pressure term in the momentum flux:

$$p = \frac{1}{2} \hat{\rho} g h^2. \tag{1.69}$$

Using this in (1.68) and canceling $\hat{\rho}$ out gives

$$(hv)_t + \left(hv^2 + \frac{1}{2} gh^2 \right)_x = 0. \tag{1.70}$$

We can combine equation (1.67), (1.70) into the system of *one-dimensional shallow water equations*

$$\begin{bmatrix} h \\ hv \end{bmatrix}_t + \begin{bmatrix} vh \\ hv^2 + \frac{1}{2} gh^2 \end{bmatrix}_x = 0 \tag{1.71}$$

Note that this is equivalent to the equations of isentropic gas dynamics (discussed in Section 1.2.1) with the value $\gamma = 2$, since setting $p(\rho) = \frac{1}{2}gh^2$ in (1.61) gives the same system.

If we assume that h and v are smooth, then equation (1.70) can be simplified by expanding the derivatives and using (1.67) to replace the h_t term. Then several terms drop out, and (1.70) is reduced to

$$v_t + \left(\frac{1}{2}v^2 + gh\right)_x = 0. \tag{1.72}$$

This equation is equivalent to the previous set (1.71) for smooth solutions, but it is important to note that the manipulations performed above depend on smoothness. For problems with shock waves, the two sets of conservation laws are not equivalent, and we know that it is crucial that we use the correct set in calculating shock waves. The form (1.71), which is derived directly from the original integral equations, is the correct set to use.

Since we will be interested in studying shock waves, we use the form (1.71) and take

$$q(x,t) = \left[\begin{array}{c} h \\ hv \end{array}\right] = \left[\begin{array}{c} q_1 \\ q_2 \end{array}\right],$$

$$f(q) = \left[\begin{array}{c} hv \\ hv^2 + \frac{1}{2}gh^2 \end{array}\right] = \left[\begin{array}{c} q_2 \\ \frac{(q_2)^2}{q_1} + \frac{1}{2}g(q_1)^2 \end{array}\right]. \tag{1.73}$$

For smooth solutions, these equations can equivalently be rewritten in the quasi-linear form

$$q_t + f'(q)q_x = 0, \tag{1.74}$$

where the Jacobian matrix $f'(q)$ is given by

$$f'(q) = \left[\begin{array}{cc} 0 & 1 \\ -\left(\frac{(q_2)}{q_1}\right)^2 + gq_1 & 2\frac{q_2}{q_1} \end{array}\right] = \left[\begin{array}{cc} 0 & 1 \\ -v^2 + gh & 2v \end{array}\right]. \tag{1.75}$$

The eigenvalues of $f'(q)$ are

$$\lambda_1 = v - \sqrt{gh}, \qquad \lambda_2 = v + \sqrt{gh}, \tag{1.76}$$

with corresponding eigenvectors

$$r_1 = \left[\begin{array}{c} 1 \\ v - \sqrt{gh} \end{array}\right], \quad r_2 = \left[\begin{array}{c} 1 \\ v + \sqrt{gh} \end{array}\right]. \tag{1.77}$$

Note that the eigenvalues and eigenvectors are functions of q for this non-linear system.

Remarks: The system (1.74) is called *hyperbolic* if the matrix $f'(q)$ is diagonalizable with real eigenvalues and it is called *strictly hyperbolic* if the eigenvalues are distinct.

If we wish to study waves with very small amplitude, then we can linearize these equations to obtain a linear system. Suppose the fluid is essentially at constant depth $h_0 > 0$ and moving at constant velocity v_0 (which may be zero), and let q now represent the perturbations from this constant state, so

$$q = \begin{bmatrix} h - h_0 \\ hu - h_0 v_0 \end{bmatrix} \quad \text{and} \quad q_0 = \begin{bmatrix} h_0 \\ h_0 v_0 \end{bmatrix}.$$

Then expanding the flux function and dropping terms of $\mathcal{O}(q^2)$ gives the linear system $q_t + Aq_x = 0$ where $A = f'q_0$. Hence small-amplitude waves move at the characteristic velocities $\lambda_0^1 = v_0 - c_0$ and $\lambda_0^2 = v_0 + c_0$, where $c_0 = \sqrt{gh_0}$. These waves propagate at speed $\pm c_0$ relative to the fluid. These shallow water waves should not be confused with sound waves, however. Sound does propagate in water, due to its slight compressibility, but in the shallow water equations we are ignoring this compressibility and hence ignoring sound waves. The waves we are modeling are often called *gravity waves*, since they are driven by the hydrostatic pressure resulting from gravity. They typically propagate at a speed $\sqrt{gh}$ that is much less than the speed of sound in water.

Note that λ_1 and λ_2 can be of either sign, depending on the magnitude of v relative to c. In shallow water theory the ratio

$$Fr = \frac{|v|}{c} \tag{1.78}$$

is called the *Froude number* (see subsection 1.1.2)

The wave speed $\sqrt{gh_0}$ depends on the depth of the fluid; waves in deeper water move faster. Note that within a wave the depth of the fluid varies (it is deeper at a crest than in a trough), and so we should expect the crest of a wave to propagate slightly faster than a trough. If the amplitude of the wave is very small compared to h_0 , then we can safely ignore this slight variation in speed, which is what we do in linearizing the equations. Then

all parts of the wave travel at the same speed based on the background depth h_0 , and the wave propagates with its shape unchanged. For waves with larger amplitude, however, the deformation of the wave due to differing wave speeds may be quite noticeable. In this case the linearized equations will not be an adequate model and the full nonlinear equations must be solved.

The nonlinear distortion of a wave leads to a steepening of the wave in the region where the fast-moving crest is catching up with the slower trough ahead of it (a compression wave), and a flattening of the wave (an expansion or rarefaction) in the region where the crest is pulling away from the following trough.

This behavior is familiar from watching waves break on the beach. Far from shore the waves we normally observe have a wavelength that is very small compared to the water depth, and hence they are governed by surface-wave theory rather than shallow water theory. Near the beach, however, the water depth is small enough that nonlinear shallow water theory applies. In this shallow water, the difference in h between crests and troughs is significant and the waves steepen. In fact the crest is often observed to move beyond the position of the preceding trough. At this point the assumptions of shallow water theory no longer hold, and a more complicated set of equations would have to be used to model breakers. Beyond the breaking time the depth h is triple-valued, a situation that obviously can't occur with other systems of conservation laws (such as gas dynamics) where the corresponding variable is a density that must be single-valued.

This extreme behavior of breaking waves results from the additional complication of a sloping beach. This leads to a continuous decrease in the fluid depth seen by the wave and a severe accentuation of the nonlinear effects. (The sloping beach, or more generally any variation in the bottom topography, also leads to additional source terms in the shallow water equations.) Shallow water waves in a domain with a flat bottom will typically not exhibit this type of breakers. Instead the gradual steepening of the wave due to nonlinearity would be counterbalanced by other effects such as surface tension (and also the vertical velocity, which is ignored in the one-dimensional model). Modeling these other effects would lead to higher-order derivatives

in the equations (with small coefficients) and consequently the equations would have smooth solutions for all time. When these coefficients are small, the wave can become nearly discontinuous, and the shock-wave solution to the hyperbolic system gives a good approximation to such solutions. In shallow water flow, a shock wave is often called a *hydraulic jump*

1.2.3 The Saint-Venant System

A lot of mathematical models have been developed to describe fluid flows, the most general is the Navier-Stokes equations, that are used to predict the behavior of viscous compressible/incompressible fluids in three dimensions. In practice when building a mathematical model, many assumptions are made to simplify the problem under consideration, and the most basic equations for describing the required phenomena are used. In open channel flows the most commonly used model is the shallow water system of equations, in which it is assumed that the flow is shallow with respect to the dimension of the considered framework. The basis of shallow water model is the continuity equation, corresponding to conservation of mass, and an equation of motion, as we have seen in Section (1.2.2). Additional terms may be incorporated to include other effects such as friction, geometry variation, viscosity etc. and these are referred to as the source terms which generally correspond to some form of loss or gain terms in the equations of the system.

In the case of modeling predominantly one-dimensional flows, the Saint-Venant equations are the most commonly used system for solving open channel flow problems, and these describe the gradually varied flow (see Section 1.1.1) of an incompressible inviscid fluid. The equations consist of a continuity or mass equation, and an equation of motion which is formed by applying Newton's Second law of motion along the channel.

A number of fundamental assumptions are inherent within the model and these can be summarized as follows:

- the flow is one-dimensional, the mean velocity is constant over a cross section and the water level is horizontal;

- the vertical component of the acceleration of the fluid is negligible so that the pressure variation with depth is hydrostatic;

- friction and turbulence can be represented using the same empirical laws that govern steady state flows.

Summarizing, the Saint-Venant equations are a particular case of shallow water equations described in Section (1.2.2), they are commonly used to describe physical situations such as flows in rivers or costal areas, specially the one-dimensional version is well adapted for ideal rectangular rivers. The system allows to describes the flow, at time $t \geq 0$ and at point $x \in \mathbb{R}$, through the height of water $h(t, x) \geq 0$ and the mean velocity $v(t, x) \in \mathbb{R}$, by the hyperbolic system

$$h_t + (hv)_x = 0, \tag{1.79}$$

$$(hv)_t + \left(hv^2 + \frac{gh^2}{2} \right)_x + ghZ'(x) = 0, \tag{1.80}$$

where g denotes the gravity intensity and $Z(x)$ is the bottom height, therefore $h + Z$ is the level of the water surface (in what follows, we also denote the discharge by $\breve{q} = hv$).
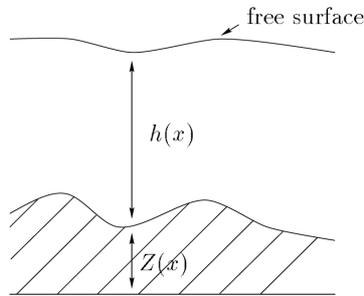

Figure 1.10: The level of water surface. (*From Ref. [1]*)

We recall some properties of the Saint-Venant system. We take them into account later in order to develop a numerical method so as to be coherent with the physical model.

First of all, the system in naturally posed for $h \geq 0$ and it is strictly hyperbolic for $h > 0$. The water height h can indeed vanish (flooding zones,

dry soils, tidal flats); this facts leads to a theoretical and numerical difficulty, because the system loses hyperbolicity at $h = 0$. (See Section 1.2.2).

The Saint-Venant system admits a mathematical *entropy*, which is also the physical energy,

$$E(h, v, Z) = \frac{hv^2}{2} + \frac{gh^2}{2} + gZh, \tag{1.81}$$

which satisfies the "entropy inequality"

$$E_t + \left[v \left(E + \frac{gh^2}{2} \right) \right]_x \leq 0. \tag{1.82}$$

Another fundamental property is related to the *stationary solutions*, that are characterized by the relations

$$\begin{aligned} hv &= C_1, \\ \tfrac{v^2}{2} + g(h + Z) &= C_2. \end{aligned} \tag{1.83}$$

Where C_1 and C_2 are two arbitrary constant. The equations (1.83) leads to several cases of special interest:

1. In the case of *stationary state* there is no motion, $v = 0$, and the water surface is flat, $h + Z = C^{st}$, for some constant C^{st}. This situation is refereed to as the *lake at rest*.

2. A *quasi-stationary state* is generated by slightly perturbing the height of the stationary state. In the one-dimensional case, assume a bottom topography in the shape of a bump and a perturbation of the form $h = C^{st} - Z + \epsilon$, where ϵ is a compactly supported perturbation. In this case the disturbance splits into two waves which, for small ϵ, are essentially linear propagating at the characteristic speeds $\pm\sqrt{gh}$ (see Section 1.2.2).

3. There are steady-states in which the momentum hv, is a nonzero constant. The different regimes of such flow depend on the bottom topography and the Froude number (see Section 1.1.2) $Fr = v/\sqrt{gh}$. If $Fr < 1$ or $Fr > 1$ everywhere, then the solution is smooth. For intermediate values of the Froude number the flow can be transcritical with transitions where Fr passes through the value 1, and hence one of

the eigenvalues, $v \pm \sqrt{gh}$ of the Jacobian, passes through zero. In this case, the steady-state solution can contain a stationary shock, called a hydraulic jumps (see Section 1.1.3).

Chapter 2

Riemann Problem for Shallow Water Equations

2.1 Dam-Break and Riemann Problems

We consider the shallow water equations (1.71) with piecewise-constant initial data

$$h(x,0) = \begin{cases} h_l & \text{if} \quad x < 0, \\ h_r & \text{if} \quad x > 0, \end{cases} \quad u(x,0) = 0, \tag{2.1}$$

where $h_l > h_r \geq 0$. This is a special case of *Riemann problem* for which $v_l = v_r = 0$, and it is called *dam-break problem* because it models what happens if a dam separating two levels of water bursts at time $t = 0$. This is the shallow water equivalent of the shock-tube problem of gas dynamics. We assume $h_r > 0$. Figure (2.1) shows the evolution of the depth and fluid velocity for the dam-break problem with data $h_l = 3$ and $h_r = 1$. Figure (2.2) shows the structure of this solution in the $x - t$ plane. Water flows from left to right in a wedge that expands from the dam location $x = 0$. At the right edge of this wedge, moving water with some intermediate depth h_m and velocity $v_m > 0$ slams into the stationary water with $h = h_r$, accelerating it instantaneously through a shock wave. The water is accelerated away from the deeper stationary water through the structure of a centered rarefaction wave.

Figure 2.1: Solution of the dam-break Riemann problem for the shallow water equation with $v_l = v_r = 0$. On the left is the depth h and on the right is the momentum hv. (*From Ref. [5]*)

The shallow water equations are a system of two equations, and so the Riemann solution contains two waves. For the case of the dam-break problem ($v_l = v_r = 0$), these always consist of one shock and one rarefaction wave. Figure (2.2) shows the structure of the exact similarity solution of this Riemann problem, along with particle paths in $x - t$ plane. Note that the fluid is accelerated smoothly through the rarefaction wave and abruptly through the shock. The formulas for this solution will be worked out in next sections.

Figure (2.3) shows the characteristic structure of the dam-break problem with data (2.1) in the case $h_l > h_r$. Figure (2.3a) shows typical characteristic curves satisfying $\frac{dX}{dt} = \lambda_1 = v - \sqrt{gh}$ (called 1-characteristics), while Figure (2.3b) shows the 2-characteristic curves satisfying $\frac{dX}{dt} = \lambda_2 = v + \sqrt{gh}$. Note that each characteristic direction is constant (the curves are straight lines) in each wedge where $q = hv$ is constant (see Section 1.2.2).

In Figure (2.3a) we see that the 1-characteristics behave near the 1-rarefaction wave just as we would expect from the nonlinear scalar case.
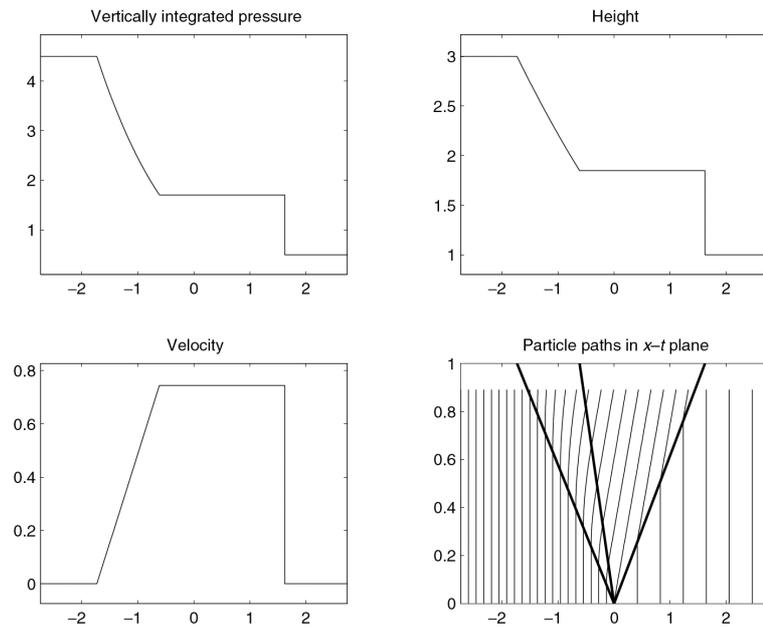
Figure 2.2: Structure of the similarity solution of the dam-break Riemann problem for the shallow water equation with $v_l = v_r = 0$. The depth h, velocity v, and vertically integrated pressure are displayed as function of $\frac{x}{t}$. The structure in the $x-t$ plane is also shown with particle path indicated for a set of particles with the spacing between particles inversely proportional to the depth. (*From Ref. [5]*)
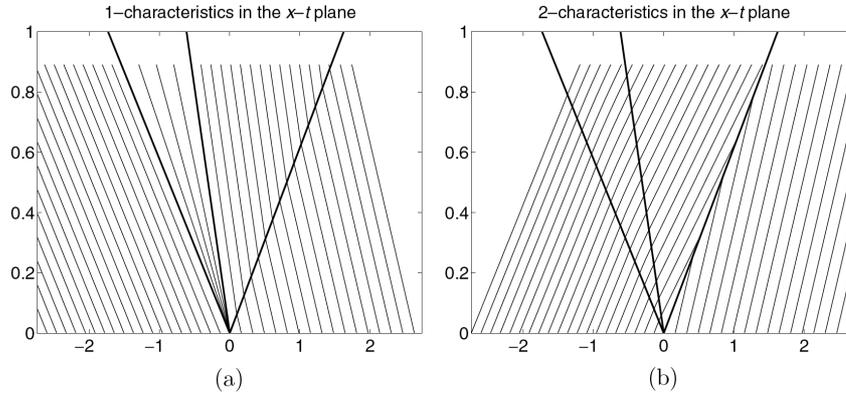
Figure 2.3: Solution of the dam-break Riemann problem for the shallow water equation show in $x - t$ plane. The dark lines shown the shock wave and the edges of the rarefaction wave seen in Figure (2.1). The lighter lines show 1-characteristic and 2-characteristics. (*From Ref. [5]*)

They spread out through the rarefaction wave, and the edges of this wave move with the characteristic velocity in each constant region bounding the rarefaction. Also note that the 1-characteristics cross the 2-waves in the sense that they are approaching the 2-wave on one side (for smaller time t) and then moving away from the 2-wave on the other side, for larger t. On the other hand, 2-characteristics shown in Figure (2.3b) impinge on the 2-shock, again as we would expect from the scalar theory of hyperbolic conservation laws (refer to [4]). These characteristics cross the 1-rarefaction with a smooth change in velocity.

This is the standard situation for many nonlinear systems of equations. For a system of m equations, there will be m characteristic families and m waves in the solution to the Riemann problem. If the pth wave is a shock, then characteristics of families 1 through $p-1$ will cross the shock from left to right, characteristics of family $p+1$ through m will cross from right to left, and characteristics of family p will impinge on the shock from both sides. This classical situation is observed in many physical problems, including the Euler equations of gas dynamics, and is the case that is best understood mathematically.

The shallow water equations are strictly hyperbolic and genuinely non-

linear (see Section 1.2.2) and so the Riemann problem always consists of two waves, each of which is a shock or rarefaction. The following example shows that other combinations are possible.

Consider the Riemann data

$$h(x,0) \equiv h_0, \quad v(x,0) = \begin{cases} v_l & \text{if } x < 0, \\ -v_l & \text{if } x > 0, \end{cases} \tag{2.2}$$

If $v_l > 0$, then this corresponds to two streams of water slamming into each other, with the resulting solution shown in Figure (2.4) for the case $h_0 = 1$ and $v_l = 1$. The solution is symmetric in x with $h(-x,t) = h(x,t)$ and $v(-x,t) = -v(x,t)$ at all times. A shock wave moves in each direction, bringing the fluid to rest, since the middle state must have $v_m = 0$ by symmetry. The characteristic structure of this solution is shown in Figure (2.5). Note again that 1-characteristics impinge on the 1-shock while crossing the 2-shock, whereas 2-characteristics impinge on the 2-shock. Note that if we look at only half of the domain, say $x < 0$, then we obtain the solution to the problem of shallow water flowing into a wall located at $x = 0$ with velocity v_l . A shock wave moves out from the wall, behind which the fluid is at rest.

The numerical tests performed in Chapter (3) refer to the physical situations described in the present chapter.

To understand the characteristic structure of the shallow water equations, it is useful to consider what happens in the solution to the Riemann problems discussed above in the case where the initial jump is so small that the linearized equation gives a good model.

Consider the data (2.1), for example, with $h_l = h_0 + \epsilon$ and $h_r = h_0 - \epsilon$ for some $\epsilon \ll h_0$. Then if we solve the Riemann problem for the linearized equation with $v_0 = 0$ in (1.75), we find that the solution consists of two acoustic waves with speeds $\pm\sqrt{gh_0}$, separated by a state (h_m, v_m) with

$$h_m = h_0, \quad v_m = \epsilon\sqrt{gh_0} \tag{2.3}$$

The solution consists of two discontinuities. If we solved the nonlinear equations with this same data, the solution would look quite similar, but the
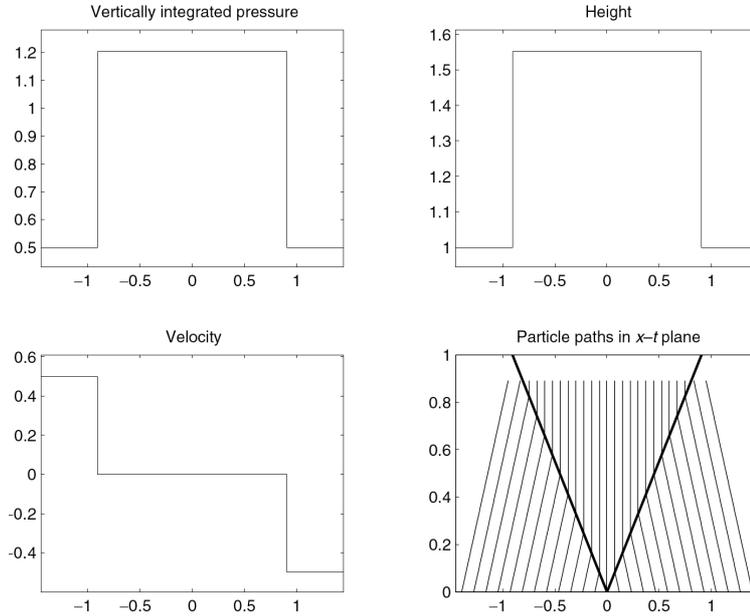
Figure 2.4: Structure of the similarity solution of the two-shock Riemann problem for the shallow water equations with $v_l = -v_r$. The depth h, velocity v, and vertically integrated pressure are displayed as functions of $\frac{x}{t}$. The structure in the $x - t$ plane is also shown with particle paths indicated for a set of particles with the spacing between particles inversely proportional to the depth. (*From Ref. [5]*)
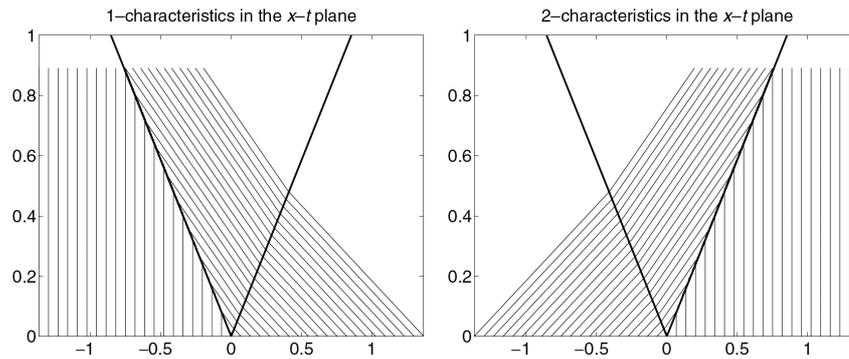

Figure 2.5: Solution of the two-shock Riemann problem for the shallow water equations, shown in the $x - t$ plane. The dark lines show the shocks. The lighter lines show 1-characteristics and 2-characteristics. (*From Ref. [5]*)

left-going wave would be a *weak rarefaction wave*, spreading very slightly with time, and with the 1-characteristics spreading slightly apart rather than being parallel as in the linear problem. The right-going wave would be a *weak shock wave*, with slightly converging characteristics.

2.2   Shock Waves and Hugoniot Loci

We consider a shallow water 2-shock such as the right-going shock in section (2.1). This shock connects some state $q_m = (h_m, h_m v_m)$ to the right state $q_r = (h_r, h_r v_r)$ from the Riemann data. We will view q_r as being fixed and determine all possible states $q = (h, hv)$ that can be connected to q_r by a 2-shock. We will find that there is a one-parameter family of such states, which trace out a curve in state space as shown in Figure (2.6b). Here the state space (phase plane) is the $h - hv$ plane. This set of states is called a *Hugoniot locus*. Which one of these possible states corresponds to q_m in the solution to the Riemann problem depends not only on q_r but also on q_l. The state q_m must lie on the curve shown in Figure (2.6b), but it must also lie on an analogous curve of all states that can be connected to q_l by a 1-wave, as determined below.

We now consider the problem of determining all states q that can be connected to some fixed state $q_* = (h_*, h_* v_*)$ (representing either q_l or q_r) by a shock. Across any shock the Rankine-Hugoniot condition must be satisfied, so for the shallow water equation, this gives a system of two equations that must simultaneously be satisfied:

$$
\begin{array}{rcl}
s(h_* - h) & = & h_* v_* - hv \\
s(h_* v_* - hv) & = & h_* v_*^2 - hv^2 + \tfrac{1}{2}g(h_*^2 - h^2),
\end{array} \tag{2.4}
$$

where s is the speed of the shock. Recall that q_* is fixed and we wish to find all states q and corresponding speeds s satisfying these relation. We thus have two equations with three unknowns, so we expect to find a one-parameter family of solutions. In fact there are two distinct families of solutions, corresponding to 1-shocks and 2-shocks. For the time being we use the term "shock" to refer to a discontinuous (weak) solution satisfying the
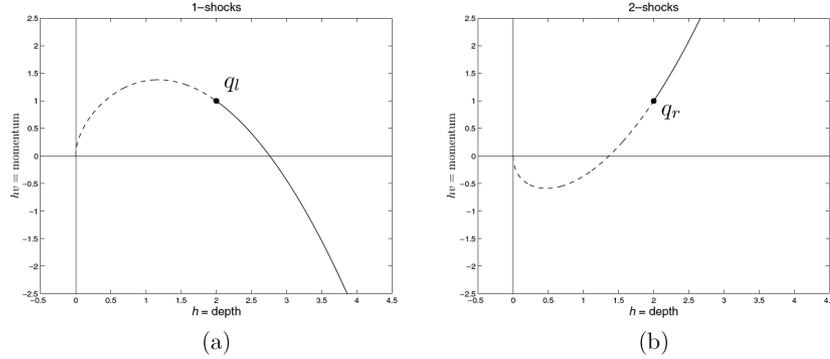
Figure 2.6: (a) Hugoniot locus of points $q = (h, hv)$ in shallow water state space that can be connected to a given state q_l by a 1-shock satisfying the Rankine-Hugoniot conditions. Only some of these states (on the solid portion of the curves) satisfy the entropy condition; see Section (2.3). (b) Hugoniot locus of points in shallow water state space that can be connected to a given state q_r by a 2-shock satisfying the Rankine-Hugoniot conditions (2.4) (*From Ref. [5]*)

Rankine-Hugoniot condition. Later we will consider the additional admissibility condition that is required to ensure that such a solution is truly a physical shock wave. There are many different ways to parameterize these families. Fairly simple formulas result from using h as the parameter. For each value of h we will determine the corresponding v and s, and plotting hv against h will give the curves shown in Figure (2.6). We first determine v by eliminating s from the system (2.4). The first equation gives

$$s = \frac{h_*}{v_* - hv} h_* - h, \tag{2.5}$$

and substituting this into the second equation gives an equation relating v to h. This is a quadratic equation in v that, after simplifying somewhat, becomes

$$v^2 - 2v_* v + \left[v_*^2 - \frac{g}{2} \left(\frac{h_*}{h} - \frac{h}{h_*} \right) (h_* - h) \right]$$

with roots

$$v(h) = v_* \pm \sqrt{\frac{g}{2} \left(\frac{h_*}{h} - \frac{h}{h_*} \right) (h_* - h)}. \tag{2.6}$$

Note that when $h = h_*$ this reduces to $v = v_*$, as we expect, since the curves we seek must pass through the point q_*. For each $h \neq h_*$ there are two different values of v, corresponding to the two families of shocks. In the case of a very weak shock ($q \approx q_*$) we expect the linearized theory to hold, and so we expect one of these curves to be tangent to the eigenvector $r_1(q_*)$ at q_* and the other to be tangent to $r_2(q_*)$. This allows us to distinguish which curve corresponds to the 1-shocks and which to 2-shocks. To see this more clearly, we multiply (2.6) by h and reparameterize by a value α, with

$$h = h_* + \alpha$$

so that $h = h_*$ at $\alpha = 0$, to obtain

$$hv = h_* v_* + \alpha \left[v_* \pm \sqrt{gh_* \left(1 + \frac{\alpha}{h_*}\right)\left(1 + \frac{\alpha}{2h_*}\right)} \right]. \qquad (2.7)$$

Hence we have

$$q = q_* + \alpha \left[\begin{array}{c} 1 \\ v_* \pm \sqrt{gh_* + \mathcal{O}(\alpha)} \end{array} \right] \quad \text{as} \quad \alpha \to 0 \qquad (2.8)$$

For α very small (as q approaches q_*), we can ignore the (α) term and we see that these curves approach the point q_* tangent to the vectors

$$\left[\begin{array}{c} 1 \\ v_* \pm \sqrt{gh_*} \end{array} \right]$$

which are simply the eigenvectors of the Jacobian matrix (1.75) at q_*. From this we see that choosing the - sign in (2.7) gives the locus of 1-shocks, while the + sign gives the locus of 2-shocks.

2.3 The Entropy condition

We consider a general Riemann problem with data q_l and q_r, and suppose we know that the solution consist of two shocks. We can then solve the Riemann problem by finding the state q_m that can be connected to q_l by 1-shock and also to q_r by a 2-shock.

We found in the previous section that though the point q_r there is a curve of points q that can be connected to q_r by a 2-shock. For a shallow water

equations, these points satisfy (2.7) with the plus sign and with $q_* = q_r$. Since q_m must lie on this curve, we have

$$h_m v_m = h_r v_r + (h_m - h_r)\left[v_r + \sqrt{gh_r\left(1 + \frac{h_m - h_r}{h_r}\right)\left(1 + \frac{h_m - h_r}{2h_r}\right)}\right],$$

which can be simplified to give

$$v_m = v_r + (h_m - h_r)\sqrt{\frac{g}{2}\left(\frac{1}{h_m} + \frac{1}{h_r}\right)}. \tag{2.9}$$

Similarly, there is a curve through q_l of states that can be connected to q_l by a 1-shock, obtained by setting $q_* = q_l$ and taking the minus sign in (2.7). Since q_m must lie on this curve, we find that

$$v_m = v_r - (h_m - h_r)\sqrt{\frac{g}{2}\left(\frac{1}{h_m} + \frac{1}{h_r}\right)}. \tag{2.10}$$

We thus have a system of two equations (2.9) and (2.10) for the two unknowns h_m and v_m. Solving this system gives the desired intermediate state in the Riemann solution. We can easily eliminate v_m from this system by noting that this appears only on the left of each equation, and the left-hand sides are equal, so equating the right-hand sides gives a single equation involving only the one unknown h_m. This can be solved by an iterative method for nonlinear equations, such as the *Newton's method.*

What happens if we apply this same procedure to a Riemann problem where the physical solution should not consist of two shocks? For example, consider the dam-break Riemann problem from section (2.1), where the solution should consist of a 1-rarefaction and a 2-shock. We can still solve the problem in terms of two "shock waves" that satisfy the Rankine-Hugoniot jump conditions, as illustrated in Figure (2.7). This gives a weak solution of the conservation laws, but one that does not satisfy the proper entropy condition for this system, as discussed in the next section. The procedure for finding the physically correct solution with a rarefaction wave is given in Section (2.5).

Figure (2.3) shows the characteristic structure for the physically correct solution to the dam-break Riemann problem from section (2.1). Figure (2.8)
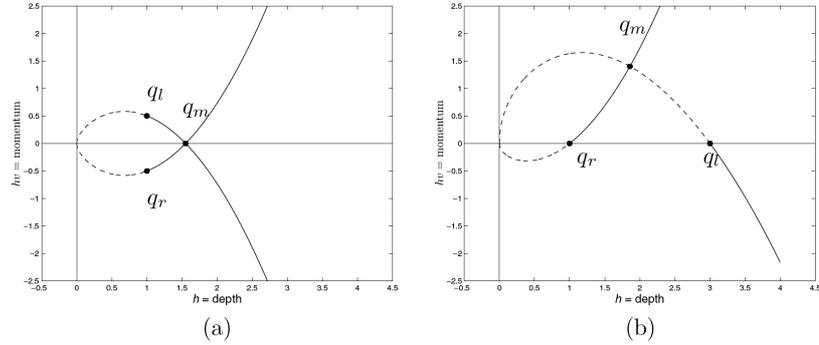
Figure 2.7: All-shock solutions to the shallow water Riemann problem can be constructed by finding the intersection of the appropriate Hugoniot loci. (a) For Riemann problem with $h_l = h_r = 1$, $v_l = 0.5$ and $v_r = -0.5$. (b) An entropy-violating Riemann solution for dam-break. (*From Ref. [5]*)

shows the structure for the weak solution for dam-break problem described at the end of previous subsection. Solution consists of two discontinuities. The 1-characteristics are not impinging on the 1-shock as they should, an indication that this structure is not stable to small perturbations and that this shock should be replaced by a rarefaction wave. This suggests the following criterion for judging whether a given weak solution is in fact the physically correct solution, a generalization of the Lax Entropy Condition to systems of equations (refer to [4]).

Lax Entropy Condition. *A discontinuity separating states* $u_l = \begin{pmatrix} h_l \\ h_l v_l \end{pmatrix}$

and $u_r = \begin{pmatrix} h_r \\ h_r v_r \end{pmatrix}$ *,propagating at speed* s*, satisfies the **Lax entropy condition** if there is an index* p *such that:* $\lambda_p(u_l) > s > \lambda_p(u_r)$*, so that p-characteristics are impinging on the discontinuity, while the other characteristics are crossing the discontinuity,*

$$\begin{aligned} \lambda_j(u_l) < s \quad and \quad \lambda_j(u_r) < s \quad for \quad j < p, \\ \lambda_j(u_l) > s \quad and \quad \lambda_j(u_r) > s \quad for \quad j > p, \end{aligned} \tag{2.11}$$

In this definition we assume the eigenvalues are ordered so that $\lambda_1 < \lambda_2 < \ldots < \lambda_m$ *in each state.*
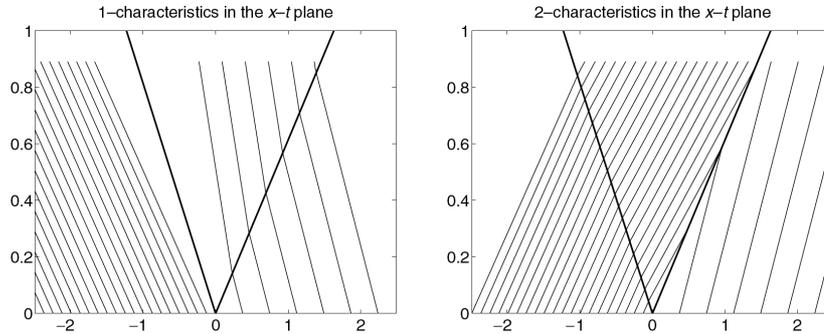
Figure 2.8: Entropy-violating solution of the dam-break Riemann problem for the shallow water equations, shown in the $x-t$ plane. The dark lines show the shocks. The lighter lines show 1-characteristics and 2-characteristics. (*From Ref. [5]*)

For the shallow water equations there is a simple criterion that can be applied to determine which parts of each Hugoniot locus give physically correct shock waves satisfying the Lax entropy condition. Across a 1-shock connecting q_l to a state q_m, we require that the characteristic velocity $\lambda_1 = v - \sqrt{gh}$ must decrease. In conjunction with the Rankine-Hugoniot condition, it can be shown that this implies that h must increase, so we require $h_m > h_l$. Similarly, a 2-shock connecting q_m to q_r satisfies the Lax entropy condition if $h_m > h_r$. Note from Figure (2.2) and Figure (2.4) that this also means that fluid particles experience an increase in depth as they pass through a shock. This is similar to the physical entropy condition for gas dynamics, that gas particles must experience an increase in physical entropy as they pass through a shock wave. Figure (2.7) shows the portions of each Hugoniot locus along which the entropy condition is satisfied as solid lines. These are simply the portions along which h is increasing. The portions indicated by dashed lines are states that can be connected by a discontinuity that satisfies the Rankine-Hugoniot condition, but not the entropy condition. We see from Figure (2.7b) that the solution to the dam-break Riemann problem consisting of two shocks fails to satisfy the entropy condition. Instead we must find a solution to the Riemann problem that consists of a 1-rarefaction and a 2-shock. In the next section we investigate rarefaction waves and

will see that the Hugoniot locus through q_l must be replaced by a different curve, the integral curve of r_1. The intersection of this curve with the 1-shock Hugoniot locus will give the correct intermediate state (h_m, v_m) for the solution.

2.4   Simple Waves and Rarefaction

In this section we will investigate solutions that are smoothly varying but which also have the property that they are associated with only one characteristic family of the system. Such waves are called *simple waves*.

In particular, the *centered rarefaction waves* that arise in the solution to Riemann problems for nonlinear systems are simple waves, but these are just one special case. They are special in that they also have the property that they are similarity solutions of the equations and are constant along every ray $\frac{x}{t} = constant$. They arise naturally from Riemann problems because of the special data used, which varies only at a single point $x = 0$, and hence all variation in the solution flows out from the point $x = t = 0$.

Let $\tilde{q}(\xi)$ be a smooth curve through state space parameterized by a scalar parameter ξ. We say that this curve is an integral curve of the vector field r_p if at each point $\tilde{q}(\xi)$ the tangent vector to the curve, $\tilde{q}'(\xi)$, is an eigenvector of $f'(\tilde{q}(\xi))$ corresponding to the eigenvalue $\lambda_p(\tilde{q}(\xi))$. If we have chosen some particular set of eigenvectors, that we call $r_p(q)$, then $\tilde{q}'(\xi)$ must be some scalar multiple of the particular eigenvector $r_p(\tilde{q}(\xi))$,

$$\tilde{q}'(\xi) = \alpha(\xi) r_p(\tilde{q}(\xi)), \tag{2.12}$$

The value of $\alpha(\xi)$ depends on the particular parameterization of the curve and on the normalization of r_p, but the crucial idea is that the tangent to the curve is always in the direction of the appropriate eigenvector r_p evaluated at the point on the curve. Figure (2.9) shows integral curves of r_1 and r_2 for the shallow water equations, for which the eigenvectors are given by (1.77). As an example of how these curves can be determined, consider r_1 and set $\alpha(\xi) \equiv 1$, which selects one particular parameterization for which
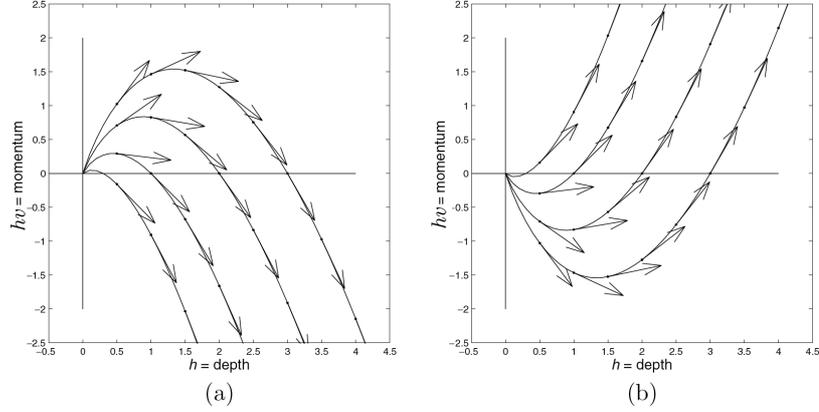
Figure 2.9: (a)Integral curves of the eigenvector r_1 for the shallow water equations. The eigenvector $r_1(q)$ evaluated at any point on a curve is tangent to the curve at that point. (b)Integrals curves for r_2 (*From Ref. [5]*)

the formulas are relatively simple. Then (2.12) reduces to

$$\tilde{q}'(\xi) = r_1(\tilde{q}(\xi)) = \left[\begin{array}{c} 1 \\ \frac{\tilde{q}_2}{\tilde{q}_1} - \sqrt{g\tilde{q}_1} \end{array} \right] \qquad (2.13)$$

by using (1.77). This gives two ordinary differential equations for the two components of $\tilde{q}(\xi)$;

$$(\tilde{q}_1)' = 1 \qquad (2.14)$$

and

$$(\tilde{q}_2)' = \frac{\tilde{q}_2}{\tilde{q}_1} - \sqrt{g\tilde{q}_1} \qquad (2.15)$$

If we set

$$\tilde{q}_1(\xi) = \xi, \qquad (2.16)$$

then (2.14) is satisfied. Note that since the first component of q is h, this means that we are parameterizing the integral curve by depth. With this choice of $\tilde{q}_1$, the second equation (2.15) becomes

$$(\tilde{q}_2)' = \frac{\tilde{q}_2}{\xi} - \sqrt{g\xi}. \qquad (2.17)$$

If we fix one point q_* on the integral curve and require that $\tilde{q}_2(h_*) = h_* u_*$, then solving the differential equation (2.17) with this initial value yields the

solution

$$\tilde{q}_2(\xi) = \xi u_* + 2\xi\left(\sqrt{gh_*} - \sqrt{g\xi}\right). \tag{2.18}$$

Plotting $(\tilde{q}_1(\xi), \tilde{q}_2(\xi))$ from (2.16) and (2.18) gives the curves shown in Figure (2.9a). Since ξ is just the depth h, we can also state more simply that the integral curves of r_1 have the functional form

$$hv = hv_* + 2h\left(\sqrt{gh_*} - \sqrt{gh}\right). \tag{2.19}$$

In terms of the velocity instead of momentum, we can rewrite this as

$$v = v_* + 2\left(\sqrt{gh_*} - \sqrt{gh}\right). \tag{2.20}$$

Similarly, the integral curve of r_2 passing though the point q_* can be shown to have the form

$$v = v_* - 2\left(\sqrt{gh_*} - \sqrt{gh}\right). \tag{2.21}$$

The expression (2.20) describes an integral curve r_1, where q_* is an arbitrary point on the curve. This can be rewritten as

$$u + 2\sqrt{gh} = v_* + 2\sqrt{gh_*}.$$

Since q_* and q are any two points on the curve, we see that the function

$$w_1(q) = v + 2\sqrt{gh} \tag{2.22}$$

has the same value at all points on this curve. This function is called *Riemann invariant* for the 1-family, or simply a 1-Riemann invariant. It is a function of q whose value is invariant along any integral curve of r_1, though it will take a different value on a different integral curve.

Similarly, from (2.22) we see that

$$w_2(q) = v - 2\sqrt{gh}, \tag{2.23}$$

is a 2-Riemann invariant, a function whose value is constant along any itegral curve of r_2.

A *simple wave* is a special solution to the conservation law in which

$$q(x, t) = \tilde{q}(\xi(x, t)), \tag{2.24}$$

where $\tilde{q}(\xi)$ traces out an integral curve of some family of eigenvectors r_p and $\xi(x,t)$ is a smooth mapping from (x,t) to the parameter ξ. This means that all states $q(x,t)$ appearing in the simple wave lie on the same integral curve. Note that any p-Riemann invariant is constant throughout the simple wave. But not every function of the form (2.24) will satisfy the conservation law. The function $\xi(x,t)$ must be chosen appropriately. We compute

$$q_t = \tilde{q}'(\xi(x,t))\xi_t \quad \text{and} \quad q_x = \tilde{q}'(\xi(x,t))\xi_x,$$

so to satisfy $q_t + f(q)_x = 0$ we must have

$$\xi_t\tilde{q}'(\xi) + \xi_x f'(\tilde{q}(\xi))\tilde{q}'(\xi) = 0.$$

Since $\tilde{q}'(\xi)$ is always an eigenvector of $f'(\tilde{q}(\xi))$, this yields

$$[\xi_t + \xi_x\lambda_p(\tilde{q}(\xi))]\tilde{q}'(\xi) = 0,$$

and hence the function $\xi(x,t)$ must satisfy

$$\xi_t + \lambda_p(\tilde{q}(\xi))\xi_x = 0. \tag{2.25}$$

Note that this is a scalar quasilinear hyperbolic equation for ξ.

In particular, if we use initial data $q(x,0)$ that is restricted entirely to this integral curve, so that $q(x,0) = \tilde{q}(\breve{\xi}(x))$ for some smooth choice of $\breve{\xi}(x)$, then (2.24) will be a solution to the conservation law for $t > 0$ provided that $\xi(x,t)$ solves (2.25) with initial data $\xi(x,0) = \breve{\xi}(x)$, at least for as long as the function $\xi(x,t)$ remains smooth. In a simple wave the nonlinear system of equations reduces to the scalar nonlinear equation (2.25) for $\xi(x,t)$.

A *centered rarefaction wave* is a special case of a simple wave, in which $\xi(x,t) = \frac{x}{t}$, so that the solution is constant on rays through the origin. A centered rarefaction wave has the form

$$q(x,t) = \begin{cases} q_l & \text{if} & \frac{x}{t} \leq \xi_1, \\ \tilde{q}\left(\frac{x}{t}\right) & \text{if} & \xi_1 \leq \frac{x}{t} \leq \xi_2, \\ q_r & \text{if} & \frac{x}{t} \geq \xi_2, \end{cases} \tag{2.26}$$

where q_l and q_r are two points on a single integral curve with $\lambda_p(q_l) < \lambda_p q_r$. This condition is required so that characteristics spread out as time advances

and the rarefaction wave makes physical sense. For a centered rarefaction wave a particular parameterization of the integral curve is forced by the fact that we set $\xi = \frac{x}{t}$. Rewriting this as $x = \xi t$, we see that the value $\tilde{q}(\xi)$ observed along the ray $\frac{x}{t}$ is propagating at speed ξ , which suggests that ξ at each point on the integral curve must be equal to the characteristic speed $\lambda_p(\tilde{q}(\xi))$ at this point. This is confirmed by noting that (2.25) in this case becomes

$$\frac{x}{t} = \lambda_p\left(\tilde{q}(\frac{x}{t})\right). \tag{2.27}$$

In particular, the left edge of the rarefaction fan should be the ray $\frac{x}{t} = \lambda_p(q_l)$ so that $\xi_1 = \lambda_p(q_l)$ in (2.26), while the right edge should be the ray $\frac{x}{t} = \lambda_p(q_r)$ so that $\xi_2 = \lambda_p(q_r)$. We thus have

$$\begin{aligned} \xi_1 &= \lambda_p(q_l), \quad \tilde{q}(\xi_1) = q_l, \\ \xi_2 &= \lambda_p(q_r), \quad \tilde{q}(\xi_2) = q_r, \end{aligned} \tag{2.28}$$

To determine how $\tilde{q}(\xi)$ varies for $\xi_1 < \xi < \xi_2$ through the rarefaction wave (2.26), rewrite (2.27) as

$$\xi = \lambda_p(\tilde{q}(\xi)) \tag{2.29}$$

and differentiate this with respect to ξ to obtain

$$1 = \nabla\lambda_p(\tilde{q}(\xi)) \cdot \tilde{q}'(\xi) \tag{2.30}$$

Using (2.12) in (2.30) gives

$$1 = \alpha(\xi)\nabla\lambda_p(\tilde{q}(\xi)) \cdot r_p(\tilde{q}(\xi))$$

and hence

$$\alpha(\xi) = \frac{1}{\nabla\lambda_p(\tilde{q}(\xi)) \cdot r_p(\tilde{q}(\xi))}. \tag{2.31}$$

Using this in (2.12) gives a system of ODEs for $\tilde{q}(\xi)$:

$$\tilde{q}'(\xi) = \frac{r_p(\tilde{q}(\xi))}{\nabla\lambda_p(\tilde{q}(\xi)) \cdot r_p(\tilde{q}(\xi))} \tag{2.32}$$

This system must be solved over the interval $\xi_1 \leq \xi \leq \xi_2$ using either of the conditions in (2.28) as an initial condition. Note that the denominator is nonzero provided that λ_p is monotonically varying. A rarefaction wave would not make sense past a point where the denominator vanishes.

Finally, for the shallow water equations (1.73) we have

$$
\begin{aligned}
\lambda_1 &= v - \sqrt{gh} = \frac{q_2}{q_1} - \sqrt{gq_1}, \\
\nabla\lambda_1 &= \begin{bmatrix} \frac{-q_2}{(q_1)^2} - \frac{1}{2}\sqrt{\frac{g}{q_1}} \\ \frac{1}{q_1} \end{bmatrix}, \\
r_1 &= \begin{bmatrix} 1 \\ \frac{q_2}{q_1} - \sqrt{gq_1} \end{bmatrix},
\end{aligned}
\tag{2.33}
$$

and hence

$$
\nabla\lambda_1 \cdot r_1 = -\frac{3}{2}\sqrt{\frac{g}{q_1}},
\tag{2.34}
$$

so that the equation of this system is

$$
\tilde{q}'(\xi) = -\frac{2}{3}\sqrt{\frac{\tilde{h}(\xi)}{g}}.
\tag{2.35}
$$

The general solution is

$$
\tilde{h} = \frac{1}{9}g(A - \xi)^2,
\tag{2.36}
$$

for some constant A. This constant must be chosen so that (2.28) is satisfied, i.e., so that $\tilde{h} = h_l$ at $\xi = v_l - \sqrt{gh_l}$ and also $\tilde{h} = h_r$ at $\xi = v_r - \sqrt{gh_r}$. Provided that q_l and q_r both lie on an integral curve of r_1, as they must if they can be joined by a centered rarefaction wave, we can satisfy both of these condition by taking

$$
A = v_l + 2\sqrt{gh_l} = v_r + 2\sqrt{gh_r}.
\tag{2.37}
$$

Recall that $v + 2\sqrt{gh}$ is a 1-Riemann invariant, which has the same value at all points on the integral curve. We see that $\tilde{h}$ varies quadratically with $\xi = \frac{x}{t}$ through a rarefaction wave (2.26).

Once we know h as a function of ξ, we can use the formula (2.21), which holds through any simple wave, to determine how v varies through the rarefaction wave. (i.e., we use the fact that the Riemann invariant is constant). Note that since we know the relation between h and v from having previously found the Riemann invariants, we do not need to solve both the ODEs in the system (2.35). We have chosen the simpler one to solve. This trick is often useful for other systems as well.

2.5   Solving the Dam-Break Problem

We start by solving the Riemann problem for which we know the solution consist of two rarefaction waves. So lets consider the shallow water equations with data (2.2), but now take $v_l < 0$. This corresponds to two streams of water that are moving apart from one another. Again the solution will be symmetric but will consist of two rarefaction waves. To solve this specific


(a)   (b)
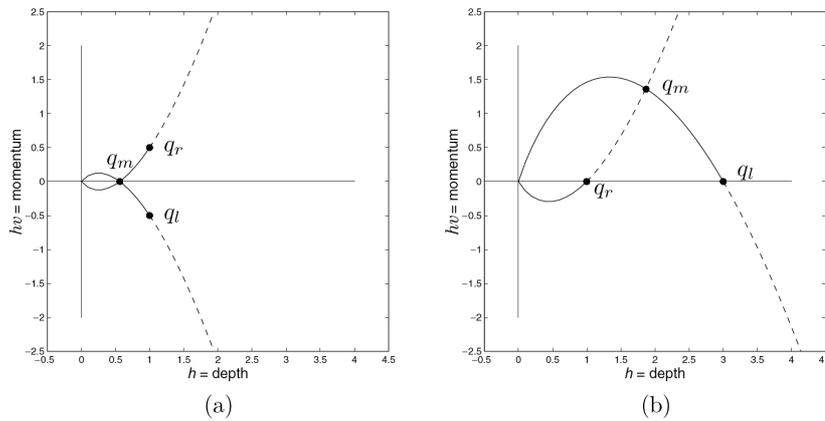
Figure 2.10: (a) Construction for a all-rarefaction Riemann solution for a problem form section (2.1). (b) The Physically incorrect all-rarefaction Riemann solution for a dam-break problem. (*From Ref. [5]*)

Riemann problem, we can proceed in a manner similar to what we did in Section (2.3) for the all-shock solution. There is an integral curve of r_1 through q_l consisting of all states that can be connected to q_l by a 1-rarefaction, and an integral curve of r 2 through q_r consisting of all states that can be connected to q_r by a 2-rarefaction. These are illustrated in Figure (2.10a) for the Riemann data

$$v_l = -0.5, \quad v_r = 0.5, \quad \text{and} \quad h_l = h_r = 1. \tag{2.38}$$

The intermediate state q_m in the Riemann solution must lie on both of these curves, and hence is at the intersection as shown in Figure (2.10a). For this particular example q_m lies on the h-axis due to symmetry. In general we can find the intersection by using the fact that q_m must lie on the curve

described by (2.20) with $q_* = q_l$ and on the curve described by (2.21) with $q_* = q_r$, so

$$v_m = v_l + 2\big(\sqrt{gh_l} - \sqrt{gh_m}\big),$$
$$v_m = v_r - 2\big(\sqrt{gh_r} - \sqrt{gh_m}\big),$$
$$(2.39)$$

This is s system of two nonlinear equations for h_m and v_m. Equating the right-hand sides gives a single equation for h_m, which can be explicitly solved to obtain

$$h_m = \frac{1}{16}g\big[v_l - v_r + 2\big(\sqrt{gh_l} + \sqrt{gh_r}\big)\big] \qquad (2.40)$$

This is valid provided that the expression being squared is nonnegative. When it reaches zero. the outflow is sufficiently great that the depth h_m goes to zero.

For the symmetric data (2.38) used in Figure (2.10a), the expression (2.40) gives $h_m = (4\sqrt{g} - 1)^2/16g = \frac{9}{16}$, since using $g = 1$. Then either equation from (2.39) gives $v_m = 0$

The integral curves in Figure (2.10a) are shown partly as dashed lines. For a given state q_l only some points on the integral curve of r_1 can be connected to q_l by a rarefaction wave that makes physical sense, since we are assuming q_l is the state on the left of the rarefaction wave. We must have $\lambda_1(q_l) < \lambda_1(q)$ for all states q in the rarefaction wave, and hence q must lie on the portion of the integral curve. Similarly, if q_r is the state to the right of a 2-rarefaction, then states q in the rarefaction must satisfy $\lambda_2(q) < \lambda_2(q_r)$ and must lie on the solid portion of the integral curve for r_2 sketched through q_r in Figure (2.10a). For the data shown in this figure, there is a state q_m that can be connected to both q_l and q_r by physically correct rarefaction waves, and the Riemann solution consists of two rarefactions.

For other data this might not be the case. Figure (2.10b) shows the data for the dam-break Riemann problem, with $h_l = 3$, $h_r = 1$, and $v_l = v_r = 0$. We can still use (2.40) to compute an intermediate state q_m lying at the intersection of the integral curves, as illustrated in Figure (2.10b), but the resulting 2-wave does not make physical sense as a rarefaction wave, since $\lambda_2(q_m) > \lambda_2(q_r)$.

Compare Figure (2.10b) with Figure (2.7b), where we found an all-shock solution to this same Riemann problem. In that case the 2-shock was acceptable, but the 1-shock failed to satisfy the entropy condition. The correct

solution consists of a 1-rarefaction and a 2-shock as shown in Figure (2.2) and determined below.

The dam-break Riemann problem for the shallow water equations has a solution that consists of a 1-rarefaction and a 2-shock, as illustrated in Figure (2.2). In Figure (2.7) we saw how to construct a weak solution to this problem that consists of two shock waves,one of which does not satisfy the Lax entropy condition. To find the correct solution we must determine an intermediate state q_m that is connected to q_l by a 1-rarefaction wave and simultaneously is connected to q_r by a 2-shock wave. The state q_m must lie on an integral curve of r_1 passing through q_l, so by (2.20) we must have

$$v_m = v_l + 2\big(\sqrt{gh_l} - \sqrt{gh_m}\big). \tag{2.41}$$

It must also lie on the Hugoniot locus of 2-shocks passing though q_r, so by (2.9) it must satisfy

$$v_m = v_r + (h_m - h_r)\sqrt{\frac{g}{2}\left(\frac{1}{h_m} + \frac{1}{h_r}\right)}. \tag{2.42}$$

We can easily eliminate v_m from these two equation and obtain a single


(a)   (b)
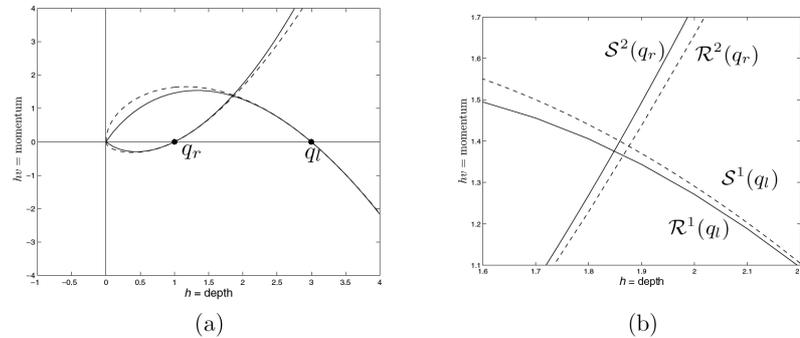
Figure 2.11: (a) The Hugoniot loci from Figure (2.7) together with the integral curves. (b) Close-up of the region where the curves intersect. $\mathcal{S}^1$: Entropy-violating 1-shocks; $\mathcal{R}^1$: 1-rarefactions; $\mathcal{S}^2$: 2-shocks: $\mathcal{R}^2$: unphysical 2-rarefactions. (*From Ref. [5]*)

nonlinear equation to solve for h_m. The structure of the rarefaction wave

connecting q_l to q_m can then be determined using theory of *Centered Rarefaction Waves*. Note that the intermediate state q_m resulting from this procedure will be slightly different from that obtained in either Figure (2.7) or Figure (2.10), since the Hugoniot loci are different from the integral curves. This is illustrated in Figure (2.11), where the curves from Figures (2.7) and (2.10) are plotted together. Figure (2.10b) shows a close-up near the points of intersection of these curves. The correct solution to the dam-break Riemann problem has the intermediate state at the point where the two solid lines cross.

2.6 The General Riemann Solver for Shallow Water equations

For the dam-break problem we know that the 1-wave is a rarefaction while the 2-wave is a shock, leading to the system of equations (2.41) and (2.42) to solve for h_m and v_m. For general values of q_l and q_r we might have any combination of shocks and rarefactions in the two families, depending on the specific data. In general, to find the state q_m we can define two functions ϕ_l and ϕ_r by

$$\phi_l(h) = \begin{cases} v_l + 2\big(\sqrt{gh_l} - \sqrt{gh}\big) & \text{if} \quad h < h_l, \\ v_l - (h - h_l)\sqrt{\frac{g}{2} - \left(\frac{1}{h} - \frac{1}{h_l}\right)} & \text{if} \quad h > h_l, \end{cases}$$

and

$$\phi_r(h) = \begin{cases} v_r - 2\big(\sqrt{gh_r} - \sqrt{gh}\big) & \text{if} \quad h < h_r, \\ v_r + (h - h_r)\sqrt{\frac{g}{2} - \left(\frac{1}{h} + \frac{1}{h_r}\right)} & \text{if} \quad h > h_r, \end{cases}$$

For a given state h, the function $\phi_l(h)$ returns the value of v such that (h, hu) can be connected to q_l through a physically correct 1-wave, while $\phi_r(h)$ returns the value such that (h, hv) can be connected to q_r through a physically-correct 2-wave. We want to determine h_m so that $\phi_l(h_m) = \phi_r(h_m)$. This can be accomplished by applying a nonlinear root finder to the function $\phi(h) \equiv \phi_l(h) - \phi_r(h)$, such as the *Newton method*.

In a scalar equation, such a Burgers equation, when two shock waves collide, they simply merge into a single shock wave with a larger jump.
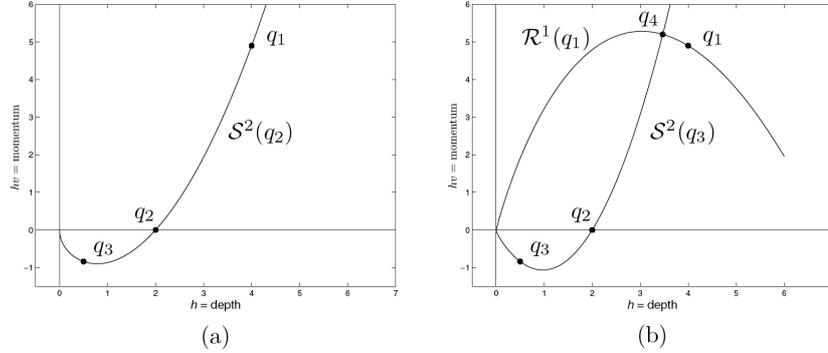
Figure 2.12: (a) Initial states q_1 and q_3 are each connected to q_2 by 2-shock. After collision, solving the Riemann problem between q_3 and q_1 gives a new state q_4 and a reflected 1-wave. (*From Ref. [5]*)

For a system of equations, the result of a *shock collision* is not so simple, even if the two shocks are in the same characteristic family. The result will include a stronger shock of this same family, but the collision will typically also introduce waves of the other families. We consider initial data for the shallow water equations (1.71) consisting of the three states shown in Figure (2.12a). These three states all lie on the Hugoniot locus $\mathcal{S}^2(q_2)$, so there is a 2-shock connecting q_1 to q_2 and a slower 2-shock connecting q_2 to q_3. If we solve the shallow water equations with data

$$q(x,0) = \begin{cases} q_1 & \text{if } x < x_1, \\ q_2 & \text{if } x_1 \le x \le x_2, \\ q_3 & \text{if } x > x_2, \end{cases} \tag{2.43}$$

for some initial shock locations $x_1 < x_2$, then the solution consists of the these two shocks, which eventually collide at some point x_c. At the time t_c when they collide, the state q_2 disappears and the solution has the form

$$q(x,t_c) = \begin{cases} q_1 & \text{if } x < x_c, \\ q_3 & \text{if } x > x_c, \end{cases} \tag{2.44}$$

To determine the solution beyond this time, note that this has the form of Riemann problem data with left state q_1 and right state q_3. The Riemann solution is not a single 2-shock, because q_1 will not lie on the Hugoniot locus

---

$\mathcal{S}^2(q_3)$. Instead, a 1-wave must be introduced to connect q_1 to a new state q_4 that lies on this Hugoniot locus, as illustrated in Figure (2.12b). We see that the 1-wave must be a rarefaction wave, since $h_4 < h_1$ and h_4 is determined by the intersection of the integral curve $\mathcal{R}^1(q_1)$ with the Hugoniot locus $\mathcal{S}^2(q_3)$.

Chapter 3

Numerical Simulation of the Shallow Water equations

3.1 Kinetic approach for the Saint-Venant System

By analogy with the Euler equations of gas dynamics, we link the Saint-Venant system to a microscopic description of the fluid and we explain how a kinetic model can be used (in general) to approximate solutions to hyperbolic conservation laws.

In the continuum description (1.80) of the fluid, the conserved quantities depth/mass, momentum, and energy are h, hv and E, respectively. This continuum description can be refined by taking the particle structure of the fluid into account. As for the case of rarefied gases, this can be done within the theory of Boltzmann equation. The basic quantity is a distribution function $f(t, x, v)$ which describes the density of particles with velocity v at position x and time t. The fluid particles move freely in space unless they undergo collisions. The corresponding evolution of f is given by a Bolzmann-type equation, namely

$$\frac{\partial f}{\partial t} + \xi \frac{\partial f}{\partial x} - gZ'(x)\frac{\partial f}{\partial \xi} = Q(t, x, \xi) \qquad (3.1)$$

The left hand side of (3.1) describes free flow of particles whereas collisions are described by the operator Q, which satisfies, for a.e. (t, x),

$$\int_{\mathbb{R}} Q d\xi = 0, \qquad \int_{\mathbb{R}} \xi Q d\xi = 0. \qquad (3.2)$$

A connection between the two descriptions (1.79)-(1.80) and (3.1) is (formally) obtained in a limit where particle collisions are dominant. In this asymptotic case, the state variables f and (h, v, E) as well as the evolutions (1.79)-(1.80) and (3.1) are equivalent. More precisely, the particle distribution function f corresponding to the macroscopic conserved quantities satisfies the following relations,

$$h \; = \; \int_{\mathbb{R}} f(h, \xi - v) d\xi, \tag{3.3}$$

$$hv \; = \; \int_{\mathbb{R}} \xi f(h, \xi - v) d\xi, \tag{3.4}$$

$$hv^2 + \frac{gh^2}{2} \; = \; \int_{\mathbb{R}} \xi^2 f(h, \xi - v) d\xi. \tag{3.5}$$

The two Saint-Venant equations are obtained by taking the moments of the kinetic equation (3.1) in $d\xi$ against 1, ξ and ξ^2 repectively: the right-hand side vanishes by (3.2) and left-hand sides coincide exactly thanks to hypothesis (3.3)-(3.5). Therefore, the non-linear shallow water system can be viewed as a single linear equation on a non-linear quantity f, for which it is easier to find simple numerical schemes with good theoretical properties. In particular, any numerical method known for the simple advection equations can directly be applied to (3.1), provided that an explicit form of the kinetic density function f is introduced.

For the numerical scheme used here, the density of particles $f(t, x, \xi)$ is given by a so-called *Gibbs equilibrium*

$$f(t, x, \xi) = f(h, \xi - v) = \sqrt{h(t, x)} \chi \left(\frac{\xi - v(x, t)}{\sqrt{h(t, x)}} \right), \tag{3.6}$$

with χ defined by

$$\chi(\omega) = \frac{\sqrt{2}}{\pi \sqrt{g}} \left(1 - \frac{\omega^2}{2g} \right)_+^{\frac{1}{2}}. \tag{3.7}$$

We also recover the energy by

$$E(h, v, Z) = \int_{\mathbb{R}} \left[\frac{\xi^2}{2} f(\xi) + \frac{\pi^2 g^2}{6} f^3(\xi) + gZ f(\xi) \right] d\xi. \tag{3.8}$$

We finally point out that that, choice of $\chi(x)$ in (3.7) is the only function such that the density (3.6) satisfies the equation

$$\xi \frac{\partial f}{\partial x} - gZ'(x)\frac{\partial f}{\partial \xi} = 0 \qquad (3.9)$$

on the steady state of the *lake at rest*

$$v(t,x) = 0, \qquad h(t,x) + Z(x) = H, \qquad \forall t \geq 0.$$

This allows to construct a consistent numerical scheme for the Saint-Venant equations with the good properties of preserving the stationary solutions as well as being endowed with a discrete entropy inequality (see Section 3.3)

3.2 Finite Volume Methods for Conservation Laws

Before we present the numerical scheme for the one-dimensional Saint-Venant system, based on the kinetic approach described in Section 3.1, it is necessary to introduce some basic concept of numerical methods for conservation laws. For the most of practical interest, it is not possible to compute an exact solutions of the shallow water equations, by using analytical techniques such as the method of characteristics. This has lead to develop to numerical methods where the continuous problem, i.e. the governing equations, is transformed into a discrete form which then results in a series of algebraic equations that can be solved on a computer. The solution to the discrete problem represents an approximation to the solution of the continuous problem and various concepts have been developed in an attempt to quantify how good the calculated numerical solution compared to the analytic solution. The following general description of basic concepts for numerical analysis of conservation laws are taken from LeVeque [6] and [5].

In one space dimension, a finite volume method is based on subdividing the spatial domain into intervals (the "finite volumes", also called *grid cells*) and keeping track of an approximation to the integral of the conserved quantities u of he model, over each of these volumes. In each time step we update these values using approximations to the flux through the endpoints of the intervals. Denote the ith grid cell by

$$C_i = (x_{i-\frac{1}{2}}, x_{i+\frac{1}{2}}),$$
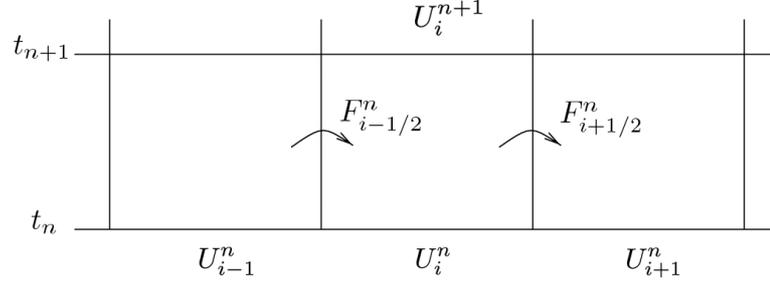
Figure 3.1: Illustration of a finite volume method for updating the cell average U_i^n by fluxes at the cell edges. Shown in $x - t$ space. (*From Ref.* [5])

as shown in Figure (3.1). The value U_i^n will be an approximation of the average value of u over i^{th} interval at time t_n:

$$U_i^n \approx \frac{1}{\Delta x} \int\limits_{x_{i-\frac{1}{2}}}^{x_{i+\frac{1}{2}}} u(x, t_n) dx \equiv \int\limits_{C_i} u(x, t_n) dx, \qquad (3.10)$$

where $\Delta x = x_{i+\frac{1}{2}} - x_{i-\frac{1}{2}}$ is the length of the cell. For simplicity we will generally assume a uniform grid, but is not required.

If $u(x, t)$ is a smooth function, by applying Taylor's theory, the integral in (3.10) agrees with the value of u at the midpoint of the interval to $\mathcal{O}(\Delta x^2)$. By working with cell averages, however, it is easier to use important properties of the conservation law in deriving numerical methods. In particular, we can insure that the numerical method is *conservative* in a way that mimics the true solution, and this is extremely important in accurately calculating shock waves. This is because $\sum_{i=1}^{N} U_i^n \Delta x$ approximates the integral of u over the entire domain of computation, and if we use a method that is in conservation form (as described below), then this discrete sum will change only due to fluxes at the boundaries of that domain. The total mass within the computational domain will be preserved, or at least will vary correctly provided the boundary conditions are properly imposed. The integral form

of the conservation law (1.23) gives:

$$\frac{d}{dt}\int_{C_i} u(x,t)dx = f(u(x_{1-\frac{1}{2}},t)) - f(u(x_{1+\frac{1}{2}},t)). \qquad (3.11)$$

We can use this expression to develop an explicit time-marching algorithm. Given U_i^n, the cell averages at time t_n , we want to approximate U_i^{n+1}, the cell averages at the next time t_{n+1} after a time step of length $\Delta t = t_{n+1} - t_n$. Integrating (3.11) in time from t_n to t_{n+1} yields

$$\int_{C_i} u(x,t_{n+1})dx - \int_{C_i} u(x,t_n)dx = \int_{t_n}^{t_{n+1}} f(u(x_{1-\frac{1}{2}},t))dt - \int_{t_n}^{t_{n+1}} f(u(x_{1+\frac{1}{2}},t))dt.$$

Rearranging this and dividing by Δx gives

$$\begin{aligned}
\frac{1}{\Delta x}\int_{C_i} u(x,t_{n+1})dx &= \frac{1}{\Delta x}\int_{C_i} u(x,t_n)dx \\
&\quad - \frac{1}{\Delta x}\left[\int_{t_n}^{t_{n+1}} f(u(x_{1+\frac{1}{2}},t))dt - \int_{t_n}^{t_{n+1}} f(u(x_{1-\frac{1}{2}},t))dt\right].
\end{aligned} \qquad (3.12)$$

This tells us exactly how the cell average of u from (3.10) should be updated in one time step. In general, however, we cannot evaluate the time integrals on the right-hand side of (3.12) exactly, since $u(x_{i\pm\frac{1}{2}},t)$ varies with time along each edge of the cell, and we do not have the exact solution to work with. This does suggest that we should study numerical methods of the form

$$U_i^{n+1} = U_i^n - \frac{\Delta t}{\Delta x}(F_{i+\frac{1}{2}}^n - F_{i-\frac{1}{2}}^n), \qquad (3.13)$$

where $F_{i-\frac{1}{2}}^n$ is some approximation to average flux along $x = x_{i-\frac{1}{2}}$:

$$F_{i-\frac{1}{2}}^n \approx \frac{1}{\Delta t}\int_{t_n}^{t_{n+1}} f(u(x_{1-\frac{1}{2}},t))dt. \qquad (3.14)$$

If we can approximate this average flux based on values U^n, then we will have a fully discrete method. See Figure (3.1) of a schematic for this process.

For a hyperbolic problem, information propagates with finite speed, so it is reasonable to first suppose that we can obtain $F_{i-\frac{1}{2}}^n$ based only on the

values U_{i-1}^n and U_i^n, the cell averages on either side of this interface. Then we might use a formula of the form

$$F_{i-\frac{1}{2}}^n = \mathcal{F}(U_{i-1}^n, U_i^n) \tag{3.15}$$

where $\mathcal{F}$ is some *numerical flux function*. The method (3.13) then becomes

$$U_i^{n+1} = U_i^n - \frac{\Delta t}{\Delta x}[\mathcal{F}(U_i^n, U_{i+1}^n) - \mathcal{F}(U_{i-1}^n, U_i^n)] \tag{3.16}$$

The specific method obtained depends on how we choose the formula $\mathcal{F}$, but in general any method of this type is an explicit method with a three-point stencil, meaning that the value U_i^{n+1} will depend on the three values U_{i-1}^n, U_i^n and U_{i+1}^n at the previous time level. Moreover, it is said to be in *conservation form*, since it mimics the property (3.12) of the exact solution. Note that if we sum $\Delta x U_i^{n+1}$ from (3.13) over any set of cells, we obtain

$$\Delta x \sum_{i=1}^N U_i^{n+1} = \Delta x \sum_{i=I}^N U_i^n - \frac{\Delta t}{\Delta x}(\hat{F}_{N+\frac{1}{2}}^n - \hat{F}_{1-\frac{1}{2}}^n). \tag{3.17}$$

In fact, the sum of the flux differences cancels out except for the fluxes at the extreme edges. Over the full domain we have exact conservation except for fluxes at the boundaries, denoted by $\hat{F}_{N+\frac{1}{2}}^n$ and $\hat{F}_{1-\frac{1}{2}}^n$, we have to define according to the model under study.

The method (3.16) can be viewed as a direct finite difference approximation to the conservation law $u_t + f(u)_x = 0$, since it gives

$$\frac{U_i^{n+1} - U_i^n}{\Delta x} + \frac{F_{i+\frac{1}{2}}^n - F_{i-\frac{1}{2}}^n}{\Delta x} = 0. \tag{3.18}$$

Many methods can be equally viewed as finite difference approximations to this equation or as finite volume methods.

There are several considerations that go into judging how good a particular flux function is for numerical computation. One essential requirement is that the resulting method should be *convergent*, i.e., the numerical solution should converge to the true solution of the differential equation as the grid is refined (as Δx, $\Delta t \to 0$). This generally requires two conditions:

- the method must be *consistent* with the differential equation, meaning that it approximates it well locally;

- the method must be *stable* in some appropriate sense, meaning that the small errors made in each time step do not grow too fast in later time steps.

The numerical flux should approximate the integral in (3.14). In particular, if the function $u(x,t) \equiv \overline{u}$ is constant in x, then u will not change with time and the integral in (3.14) simply reduces to $f(\overline{u})$. As a result, if $U^n_{i-1} = U^n_i = \overline{u}$, then we expect the numerical flux function $\mathcal{F}$ of (3.15) to reduce to $f(\overline{u})$, so we require

$$\mathcal{F}(\overline{u}, \overline{u}) = f(\overline{u}) \tag{3.19}$$

for any value $\overline{u}$. This is part of basic *consistency condition*. We generally also expect continuity in this function as U_{i-1} and U_i vary, so that $\mathcal{F}(U_{i-1}, U_i) \rightarrow f(\overline{u})$ as $U_{i-1}, U_i \rightarrow \overline{u}$. Typically some requirement of *Lipschitz continuity* is made, e.g., there exist a constant L so that

$$|\mathcal{F}(U_{i-1}, U_i) - f(\overline{u})| \leq L \max(|U_i - \overline{u}|, |U_{i-1} - \overline{u}|) \tag{3.20}$$

The so called *CFL condition*, must be satisfied by any finite volume or finite difference method if we expect it to be stable and converge to the solution of the differential equation as the grid is refined. It simply states that the method must be used in such a way that information has a chance to propagate at the correct physical speeds, as determined by the eigenvalues of the flux Jacobian $f'(u)$.

With the explicit method (3.16) the value U^n_{i+1} depends only on three values U^n_{i-1}, U^n_i, and U^n_{i+1} at the previous time step. Suppose we apply such a method to the advection equation $u_t + au_x = 0$ with $a > 0$ so that the exact solution simply translates at speed a and propagates a distance $a\Delta t$ over one time step. Figure (3.2a) shows a situation where $a\Delta t < \Delta x$, so that information propagates less than one grid cell in a single time step. In this case it makes sense to define the flux at $x_{i-\frac{1}{2}}$ in terms of U^n_{i-1} and U^n_i alone. In Figure (3.2b), on the other hand, a larger time step is used with $a\Delta t > \Delta x$. In this case the true flux at $x_{i-\frac{1}{2}}$ clearly depends on the value of U^n_{i-2}, and so should the new cell average U^{n+1}_i. The method (3.13) would certainly be unstable when applied with such a large time step, no matter
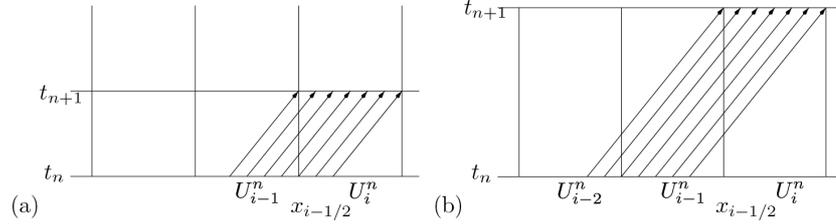
Figure 3.2: Characteristic for the advection equation, showing the information that flows into cell C_i during a single time step. (a) For a small enough time step, the flux $x_{i-1/2}$, depends only on the values in neighboring cells - only on U_{i-1}^n in this case where $a > 0$. (b) For a larger time step, the flux should depend on values father away. (*From Ref. [5]*)

how the flux (3.15) was specified, if this numerical flux depend only on U_{i-1}^n and U_i^n.

This leads to the introduction of the *CFL condition*, named after Courant, Friedrichs and Lewy [2]:

A numerical method can be convergent only if its numerical domain of dependence contains the true domain of dependence of the differential equation, at least in the limit as Δt and Δx go to zero.

It is very important to note that the CFL condition is only a *necessary* condition for stability (and hence convergence). It is not always *sufficient* to guarantee stability.

The numerical domain of dependence of a method is defined as the set of points where the initial data can possibly affect the numerical solution at any point (x, t).

In order for the CFL condition to be satisfied, the domain of dependence of the true solution must lie within computational domain. This leads to a relation between the time step Δt and space step Δx through the *Curant number*, to be checked in the implementation of the scheme.

For a hyperbolic system of equations there are generally a set of m wave speeds $\lambda_1, \ldots, \lambda_m$ where $m \in \mathbb{N}^+$ (see Section 1.2.2 for example of water

small waves). In this case we define the Courant number by

$$\nu = \frac{\Delta t}{\Delta x} \max_p |\lambda_p|. \tag{3.21}$$

For a three-point method the CFL condition leads to a necessary condition $\nu \leq 1$. Note that if the method has a wider stencil, then the CFL condition will lead to a more lenient condition on the time step.

For hyperbolic equations we typically use explicit methods and grids for which the Courant number is somewhat smaller than 1. This allows keeping $\frac{\Delta t}{\Delta x}$ fixed as the grid is refined, which is sensible in that generally we wish to add more resolution at the same rate in both space and in time in order to improve the solution.

3.3   Kinetic scheme for the Saint-Venant System

We introduce a finite volume scheme for the one-dimensional Saint-Venant system, based on the kinetic approach described in Section 3.1, that is taken from Perthame, Simeoni [7].

If $Z(x)$ is the function describing the bottom height, the cell averages are given by $Z_i = \frac{1}{\Delta x} \int_{C_i} Z(x)dx$. Starting from the microscopic equation (3.1), we perform a discretization directly on the density of particles

$$f_i^{n+1}(\xi) - f_i^n(\xi) + \frac{\Delta t}{\Delta x}\xi\left(f_{i+\frac{1}{2}}^-(\xi) - f_{i-\frac{1}{2}}^+(\xi)\right) = 0, \tag{3.22}$$

where the interface densities $f_{i+\frac{1}{2}}^\pm$ are defined later. As usual, the "collision term" $Q(x,t,\xi)$ in the kinetic representation, which relaxes the kinetic density f to a *Gibbs equilibrium* (3.6), is neglected in the numerical scheme; at each time-step we project $f_i^n(\xi)$ on the equilibrium, which is way to performe all collisions at once and to recover the *Gibbs equilibrium* without computing it.

Note that the fluxes can also be written as

$$f_{i+\frac{1}{2}}^-(\xi) = f_{i+\frac{1}{2}}(\xi) + \left(f_{i+\frac{1}{2}}^-(\xi) - f_{i+\frac{1}{2}}(\xi)\right) \tag{3.23}$$

and the quantity $\delta f_{i+\frac{1}{2}}^-(\xi) = f_{i+\frac{1}{2}}^-(\xi) - f_{i+\frac{1}{2}}(\xi)$ holds for the discrete contribution of the source term $hZ'(x)$ in the system, for negative velocities;

indeed, $\delta f_{i+\frac{1}{2}}^{-}(\xi) = 0$ for $\xi \geq 0$ in the scheme below. This is the principle of *interfracial upwind sources*: the source is not treated as a volumic term but at the interfaces and it is upwinded.

Now, we integrate Eq. (3.22) in $d\xi$ against 1 and ξ, with notation

$$U_i^{n+1} = (h_i^{n+1}, (hu)_i^{n+1}),$$

$$h_i^{n+1} = \int_{\mathbb{R}} f_i^{n+1}(\xi)d\xi, \qquad (hu)_i^{n+1} = \int_{\mathbb{R}} \xi f_i^{n+1}(\xi)d\xi$$

and obtain the macroscopic scheme

$$U_i^{n+1} - U_i^n + \frac{\Delta t}{\Delta x}\left[\mathbb{F}_{i+\frac{1}{2}}^{-} - \mathbb{F}_{i-\frac{1}{2}}^{+}\right] = 0. \qquad (3.24)$$

The numerical fluxes are thus given by the kinetic fluxes

$$\mathbb{F}_{i+\frac{1}{2}}^{-} = \int_{\mathbb{R}} \xi \begin{pmatrix} 1 \\ \xi \end{pmatrix} f_{i+\frac{1}{2}}^{-}(\xi)d\xi, \qquad (3.25)$$

$$\mathbb{F}_{i-\frac{1}{2}}^{+} = \int_{\mathbb{R}} \xi \begin{pmatrix} 1 \\ \xi \end{pmatrix} f_{i-\frac{1}{2}}^{+}(\xi)d\xi. \qquad (3.26)$$

In order to take the neighboring cells into account in a natural interpretation of the microscopic features of the system, we formulate a peculiar discretization for the fluxes in (3.22), computed by the upwind formulas

$$f_{i+\frac{1}{2}}^{-}(\xi) = f_i^n(\xi)\mathbb{I}_{\xi\geq0} + f_{i+\frac{1}{2}}^n(\xi)\mathbb{I}_{\xi\leq0}, \qquad (3.27)$$

$$f_{i-\frac{1}{2}}^{+}(\xi) = f_{i-\frac{1}{2}}^n(\xi)\mathbb{I}_{\xi\geq0} + f_i^n(\xi)\mathbb{I}_{\xi\leq0}, \qquad (3.28)$$

where we define

$$
\begin{aligned}
f_{i+\frac{1}{2}}^n(\xi) &= f_i^n(-\xi)\mathbb{I}_{|\xi|^2\leq2g\Delta Z_{i+\frac{1}{2}}} \\
&+ f_{i+\frac{1}{2}}^n\left(-\sqrt{|\xi|^2 - 2g\Delta Z_{i+\frac{1}{2}}}\right)\mathbb{I}_{|\xi|^2\geq2g\Delta Z_{i+\frac{1}{2}}}, \\
f_{i-\frac{1}{2}}^n(\xi) &= f_i^n(-\xi)\mathbb{I}_{|\xi|^2\leq2g\Delta Z_{i-\frac{1}{2}}} \\
&+ f_{i-\frac{1}{2}}^n\left(\sqrt{|\xi|^2 - 2g\Delta Z_{i-\frac{1}{2}}}\right)\mathbb{I}_{|\xi|^2\geq2g\Delta Z_{i-\frac{1}{2}}},
\end{aligned}
$$

Where $\Delta Z_{i+\frac{1}{2}} = Z_{i+1} + Z_i$ and $\Delta Z_{i-\frac{1}{2}} = Z_i - Z_{i-1}$.
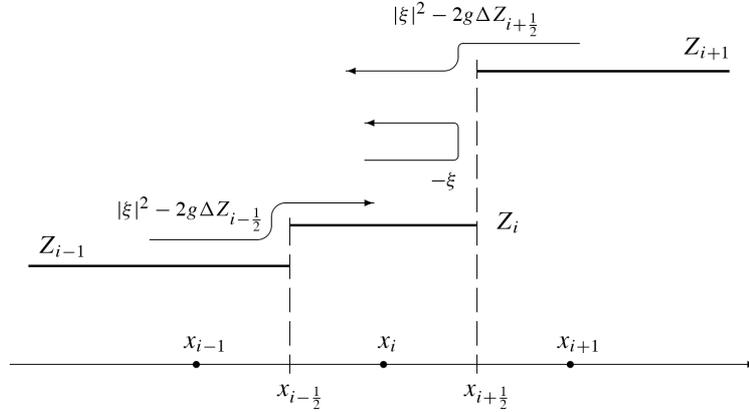
Figure 3.3: Illustration of the typical sytuation occuring in a celll C_i of the mesh, centered at the point $x_i \in \mathbb{R}$. (*From Ref. [7]*)

The figure (3.3) illustrates the typical situation occurring in a cell C_i of the mesh, centered at the point $x_i \in \mathbb{R}$; without loss of generality, we consider here the case of an interesting bottom slope, so that the bottom jumps are positive and negative for neighboring cells C_{i-1} and C_{i+1} respectively.

The effect of the source term is made explicit by treating it as a physical potential. The definitions (3.27)-(3.28) are thus a mathematical formalization which describes the physical microscopic behavior of the system: contributions to the value $f_i^{n+1}(\xi)$ are also given by the particles in C_{i+1} and in C_{i-1} at time t_n, with kinetic energy sufficient to surpass the potential difference (speeded up or down though the potential jump) and by particles coming at velocity $-\xi$, reflected on the bottom jumps according to classical mechanics, when their energy is too small (i.e., $|\xi|^2 \leq 2g\Delta Z_{i+\frac{1}{2}}$). We see immediately that the kinetic scheme (3.24)-(3.26) is water height conservative.

In fact, still referring to the figure, we compute the first component of the numerical fluxes at the interface $x_{i+\frac{1}{2}}$ of the mesh by the formulas

(3.25)-(3.26),

$$
\begin{aligned}
(\mathbb{F})_{i+\frac{1}{2}}^{-} &= \int\limits_{\xi \geq 0} \xi f_i^n(\xi) d\xi + \int\limits_{\xi \leq 0} \xi f_i^n(-\xi) \mathbb{I}_{|\xi|^2 \leq 2g\Delta Z_{i+\frac{1}{2}}} d\xi \\
&+ \int\limits_{\xi \leq 0} \xi f_i^n \left(-\sqrt{|\xi|^2 - 2g\Delta Z_{i+\frac{1}{2}}} \right) \mathbb{I}_{|\xi|^2 \leq 2g\Delta Z_{i+\frac{1}{2}}} d\xi
\end{aligned}
$$

and

$$
(\mathbb{F})_{i+\frac{1}{2}}^{+} = \int\limits_{\xi \leq 0} \xi f_{i+1}^n(\xi) d\xi + \int\limits_{\xi \geq 0} \xi f_i^n \left(\sqrt{|\xi|^2 - 2g\Delta Z_{i+\frac{1}{2}}} \right) d\xi,
$$

so that a simple change of variable $|\xi'|^2 = |\xi|^2 - 2g\Delta Z_{i+\frac{1}{2}}$, $\xi' d\xi' = \xi d\xi$ allow us to conclude that

$$
(\mathbb{F}_h)_{i+\frac{1}{2}}^{-} = (\mathbb{F}_h)_{i+\frac{1}{2}}^{+}, \qquad \forall i \in \mathbb{Z}.
$$

The conservation of water height and momentum is also obvious for the system with flat bottom: the continuous system (1.79)-(1.80) becomes homogeneous ($Z'(x) = 0$) and we obtain a conservative scheme, with the flux-splitting form of the standard kinetic scheme.

Remark: We emphasize that demonstrating the numerical scheme (3.24)-(3.26) to be consistent can not be achieved in the classical manner. Because of the presence of the source term and the decision to process it implicitly.

We state here theoretical properties of the numerical scheme introduced above, which represent the discrete analogues of the main properties of the Saint-Venant system stated in Section 1.2.3. We refer to [7] for the proof.

We assume the CFL condition,

$$
\Delta t \max \left(|v_i^n| + \sqrt{2gh_i^n} \right) \leq \Delta x. \tag{3.29}
$$

Then,

1. the kinetic scheme (3.24)-(3.26) keeps the water height positive, i.e., $h_i^n \geq 0$ if this was the case initially;

2. it satisfies the conservative in-cell entropy inequality,

$$
E_i^{n+1} - E_i^n + \frac{\Delta t}{\Delta x} \left[\eta_{i+\frac{1}{2}}^n - \eta_{i-\frac{1}{2}}^n \right] \leq 0,
$$

with the discrete entropy fluxes

$$
\begin{aligned}
\eta_{i+\frac{1}{2}}^n &= \int\limits_{\xi \geq 0} \left[\frac{\xi^3}{2} M_i^n(\xi) + \frac{\pi^2 g^2}{6} \xi [M_i^n(\xi)]^3 + g Z \xi M_i^n(\xi) \right] d\xi \\
&+ \int\limits_{\xi \leq 0} \left[\frac{\xi^3}{2} M_{i+\frac{1}{2}}^n(\xi) + \frac{\pi^2 g^2}{6} \xi [M_{i+\frac{1}{2}}^n(\xi)]^3 + g Z \xi M_{i+\frac{1}{2}}^n(\xi) \right] d\xi, \\
\eta_{i-\frac{1}{2}}^n &= \int\limits_{\xi \geq 0} \left[\frac{\xi^3}{2} M_{i-\frac{1}{2}}^n(\xi) + \frac{\pi^2 g^2}{6} \xi [M_{i-\frac{1}{2}}^n(\xi)]^3 + g Z \xi M_{i-\frac{1}{2}}^n(\xi) \right] d\xi \\
&+ \int\limits_{\xi \leq 0} \left[\frac{\xi^3}{2} M_i^n(\xi) + \frac{\pi^2 g^2}{6} \xi [M_i^n(\xi)]^3 + g Z \xi M_i^n(\xi) \right] d\xi.
\end{aligned}
$$

and the discrete energy

$$
E_i^n = h_i^n \frac{|v_i^n|^2}{2} + \frac{g(h_i^n)^2}{2} + g Z_i h_i^n;
$$

3. the scheme (3.24)-(3.26) preserves the steady states of the system given by a lake at rest,

$$
v_i^n = 0, \quad h_i^n + Z_i = H, \qquad \forall i \in \mathbb{Z}, \qquad \forall n \in \mathbb{N}.
$$

To proceed to the actual implementation of the scheme (3.24)-(3.26), we have to compute the numerical fluxes explicitly. Since their expressions are not always immediate to calculate, it is necessary to use an approximation technique for some of them. We refer to to [7] for the details.

3.4 Numerical Tests

We conclude this chapter with numerical examples that illustrate the results stated in the previous sections and we check the properties of the scheme on different test cases for which analytical solutions of the equations are available (see Chapter 2). For each test, the channel length is $L = 200m$ and the computational domain is chosen to be symmetric around the point $x = 0$, the mesh size is $\Delta s = L/100$ and the time-step Δt is computed according to the CFL condition (3.29).

3.4.1   Dam Break

We begin with a Dam-Break test in a rectangular channel with flat bottom $(Z = 0)$. The initial conditions are

$$
\begin{aligned}
v(0, x) &= 0 \\
h(0, x) &= \left\{ \begin{array}{ll} h_l & \text{for} \quad x \leq 0 \\ h_r & \text{for} \quad x > 0, \end{array} \right.
\end{aligned}
$$

where $h_l > h_r$ in order to be consistent with the physical phenomenon of a Dam-Break from the left to the right. Note that this case corresponds to a Riemann problem described in Section (2.1) Figures (3.4) and (3.5) presents the results observed at time $t = 0s$ and $t = 120s$, for a Dam-Break on a wet bed $(h_l = 4.0m, h_r = 1.25m)$.
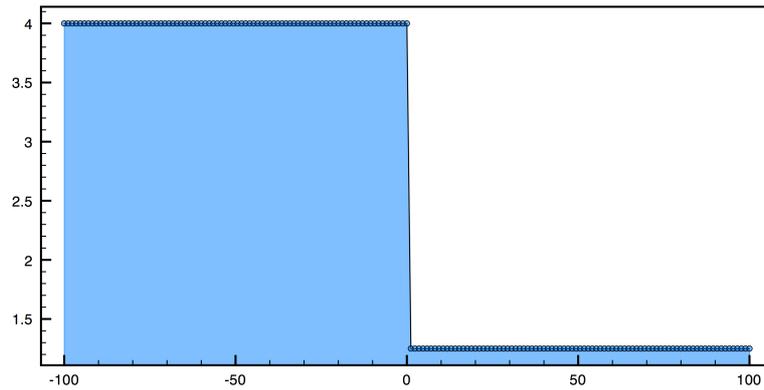
Figure 3.4: Numerical Test: Dam break on a wet bed - initial water level.
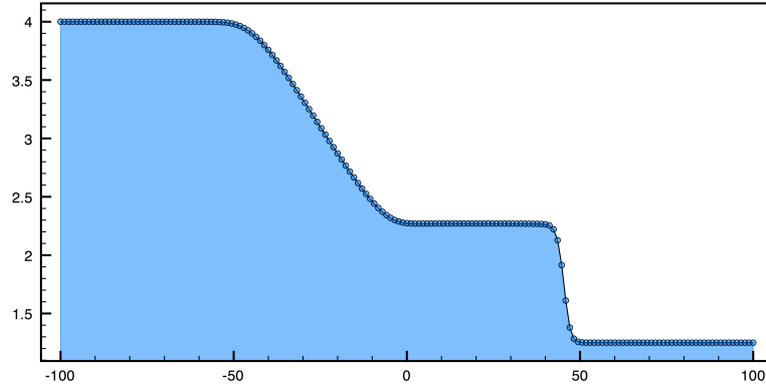
Figure 3.5: Numerical Test: Dam break on a wet bed - final water level.

3.4.2 Small perturbation

We now consider a test case concerning the small perturbation on water surface, over flat bottom. This situation is related to discussion about linearization for shallow water equations form Section (1.2.2). Figures (3.6) presents the initial water level with small rectangular projection, symmetric around the point $x = 0$ and the Figure (3.7) presents the results observed at time $t = 120s$.
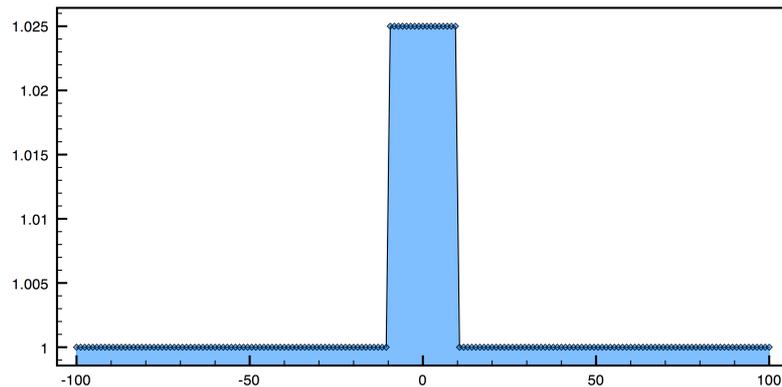

Figure 3.6: Numerical Test: Small perturbation - initial water level.
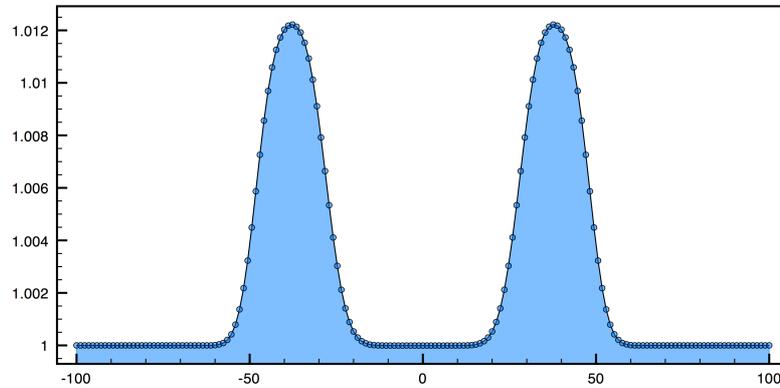
Figure 3.7: Numerical Test: Small perturbation - final water level

3.4.3 Perturbation over bump

At the end, we consider the perturbation over bump. Unfortunately this case leads to improper semi-stationary solution. The water level rapidly takes shape similar to the bottom topography and then, very slowly loses height. The problem is hidden in implementation of boundary condition and it will be a subject of a future investigation. Figures (3.8) and (3.9) presents the results observed at time $t = 0s$ and $t = 250s$

3.5 Program description

The original version of the program consisted of a simple console program written in *GNU Fortran 77* and reproducing the numerical scheme described in (3.3). The first issue has been to understand the code structure and execute that version under different operating systems (*Windows XP, Linux*). Also the idea arose to build a suitable graphical interface, in order to help users to edit configuration files and execute the base program by automatic button press. The next step has been to add plotting functionalities and to automatically produce sequences of pictures to be combined as
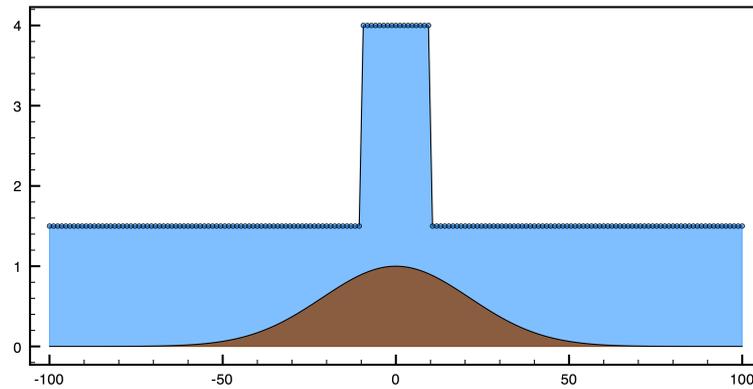
Figure 3.8: Numerical Test: Perturbation over bump - initial water level.
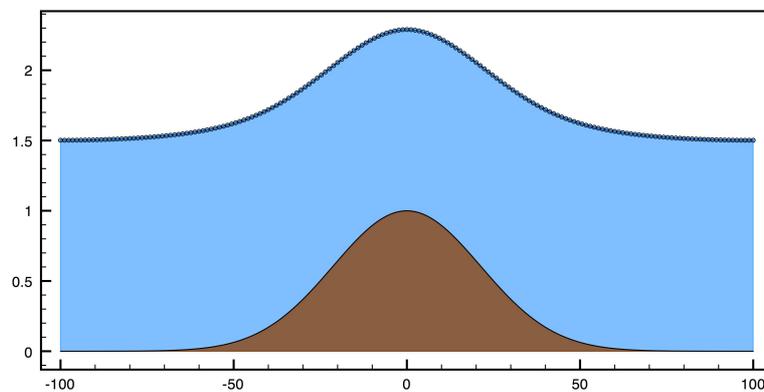
Figure 3.9: Numerical Test: Perturbation over bump - final water level

a movie.

The interface is written in *Java*, and then it turns out to be Operating System independent. It is an extension of the Fortran base program and it is not mandatory for executing numerical tests. Figure (3.10) shows a schematic view of the program structure. The interface communicates with the base program through the configuration file - "svk.data", the macro configuration file for $PLOT$ program - "macro.tmp", and set of parameters (added at the end of the configuration file) that are used to make animations. Figure (3.12) shows the program in action with the windows open for each program module. In the case when the $PLOT$ program is not available on the computer, the base program skips plot and animation process and it just writes the output data in series of **.dat* files (more informations about using the program can be found in the PDF version of the user guide inside the CD jointed to the present manuscript). The scheme of interface that we
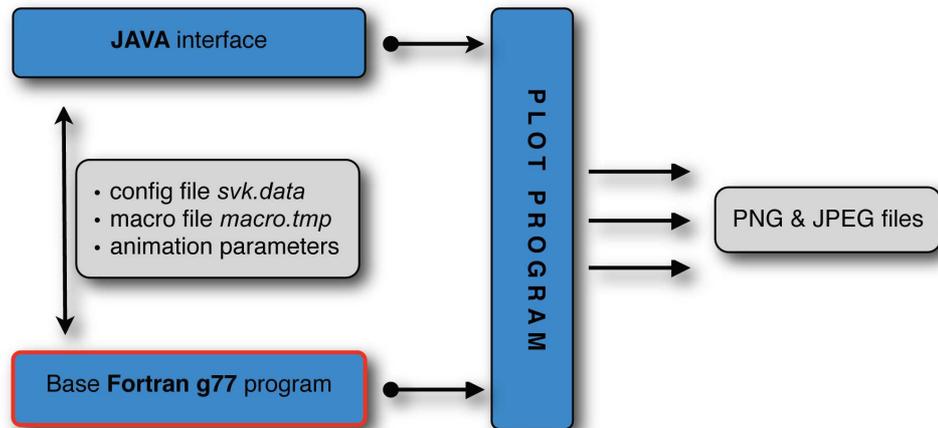

Figure 3.10: Scheme of program modules.

have realized is not, however, completely robust. It helps the users to achieve some functionalities (plotting data during the computation, quick changing parameters of simulation, etc.), but each call of an external module through the layer of the operating system (showed as black arrows in Fig. (3.10)) is

time consuming and makes difficult to catch errors, so that an alternative solution is recommended.

For better performance and compatibility with various plotting, interface and programing libraries, we suggest to rewrite the base program/code in $C++$ language, and then to implement an interface and plotting functionality by using *Trolltech QT4* libraries. The *Trolltech QT4* is fully operating system independent, and desired interfaces can be easily designed by *QT4 Designer*. Moreover, the *QT4 system* consists of useful graphical libraries which can be used to build plotting functions. Figure (3.11) presents
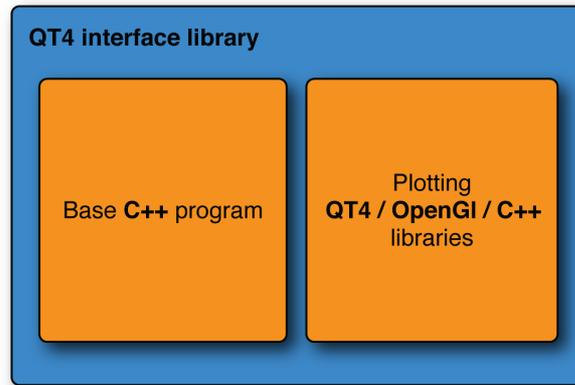

Figure 3.11: Proposition scheme of program architecture.

a scheme of program rewritten in $C++$. The plot and base code modules are not in separated programs, but they are build-in functions inside the *QT4* interface program. This solution leads obviously to better performance and controllability.
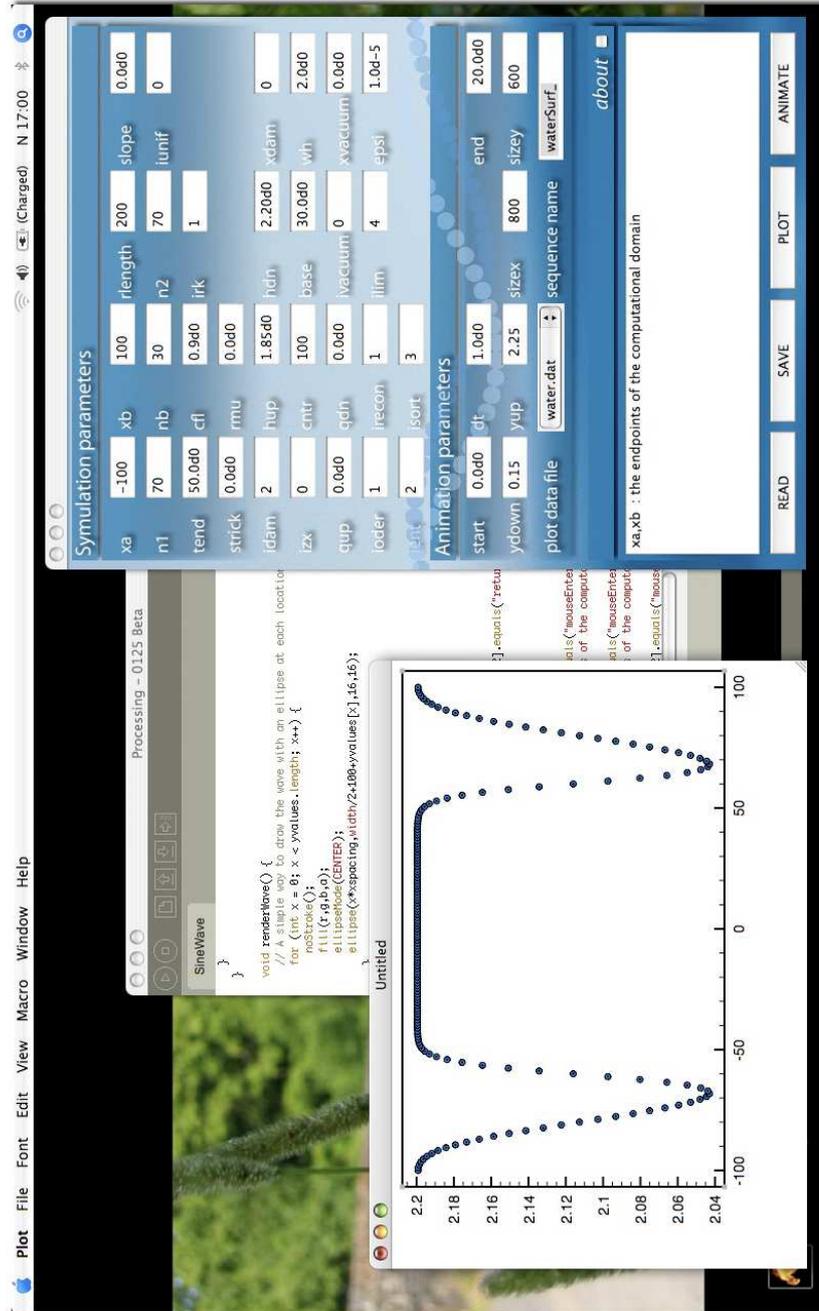
Figure 3.12: Program in action, under MacOSX - operating system

Bibliography

[1] E. Adusse, M. Bristeau and B. Perthame, *Kinetic scheme for Saint-Venant equations with source terms on unstructed grids*, INRIA J. no. 3989, Juillet 2000

[2] R. Courant, K. O. Friedrichs, and H. Lewy, *On the partial difference equations of mathematical physics*, IBM J., 11(1967), pp.215-234.

[3] M. Junk, *A new perspective on kinetic schemes*, SIAM J. Numer. Anal. 38(2000), no. 5, pp.1603-1625

[4] P. D. Lax, *Hyperbolic systems of conservation laws and the mathematical theory of shock laws*, in Regional Conf. Ser. in Appl. Math. 11, SIAM, Philadelphia, 1973

[5] R. J. LeVeque, *Finite Volume Methods for Hyperbolic Problems*, Cambridge Texts in Applied Mathematics, Cambrige 2004

[6] R. J. LeVeque, *Numerical methods for conservation laws*, Lectures in Mathematics ETH Zürich, Birkhäuser Verlag, Basel, 1990

[7] B. Perthame, C. Simeoni, *Kinetic scheme for the Saint-Venant system with a source term*, Calcolo, 38(4), pp.201-231, 2001

[8] R. Puzyrewski, J. Sawicki, *Podstawy mechaniki płynów i hydrauliki.* Wydawnictwo Naukowe PWN, Warszawa, 2000

[9] Frank M. White, *Fluid Mechanics* Mc-Graw-Hill, Fourth Edition, 1999

[10] G. Whitham, *Linear and Nonlinear Waves*, Wiley-Interscience, New York, 1974